The Effects of Proton Radiation on HfO_2-based RRAM

By

Panpan Xue

A dissertation submitted in partial fulfillment of

the requirements for the degree of

Doctor of Philosophy

(Electrical and Computer Engineer)

at the

UNIVERSITY OF WISCONSIN-MADISON

2018

Date of final oral examination: 12/21/2018

The dissertation is approved by the following members of the Final Oral Committee:

J. Leon Shohet, Professor, Electrical and Computer Engineering
Zhenqiang Ma, Professor, Electrical and Computer Engineering
Yu Hen Hu, Professor, Electrical and Computer Engineering
Yoshio Nishi, Professor, Electrical Engineering, Stanford University, was affiliate of Materials Science and Engineering

The effects of proton radiation on HfO_2-based RRAM

Panpan Xue

Under the supervision of Professor J. L. Shohet

at the University of Wisconsin-Madison

Abstract

Hafnium oxide(HfO_2) is one of the most popular dielectric materials for RRAM. Cosmic ray is a major radiation damage and contains about 90% proton. In order for HfO_2-based RRAM to considered using in space related application, it is important to investigate the effects of proton radiation on HfO_2-based RRAM. Changes of the defect concentrations of HfO_2 may affect the resistive-switching mechanism of RRAM. In this work, in order to investigate the effects of proton radiation on HfO_2-based RRAM, HfO_2-based RRAM cells and HfO_2 blanket film are exposed to proton radiation with energy from 10-keV to 300-keV, fluence from 10^9 to 10^{15} photons/cm^2. After proton radiation, I-V characteristics are measured with pristine and proton-irradiated RRAM cells as function of proton energy and proton fluence. Some of the 10keV proton-irradiated RRAM cells are formed during proton irradiation and turn to LRS. The HRS resistance decreased after proton irradiation. The ESR, C-V measurements are made with HfO_2 blanket films. The results show that oxygen vacancies are generated in the bulk of HfO_2 and the interface, from displacement damage. The extra radiation-induced oxygen vacancies increase the conductive filaments' size and length

and decrease the HRS resistance. This is consistent with TRIM code simulation results. Then, the endurance of proton irradiated RRAM cells are measured as a function of proton energy, fluence and temperature. The endurance cycles decrease with higher proton energy and also decrease when the proton fluence are higher than 10^{13} cm^{-2}. The retention time measurements show that after proton irradiation with energy from 10keV to 300keV, the HfO_2-based RRAM can still maintain the stored information for about 14-15 years.

Approved:

December 23, 2018

Date

Professor J. L. Shohet

Acknowledgements

During my studies at the University of Wisconsin-Madison, I have had the honor of working with many people who have influenced me greatly. I am indebted to the many professors, colleagues, and friends who have helped me along the path to completing my Ph.D.

I would like to thank my advisor, Professor J. Leon Shohet, for his 6 years of guidance, patient and help. He teaches me not only knowledges but more importantly how to learn and do research. During my years of study in plasma processing technology lab, I have benefitted greatly from his support, guidance, advice and all his encouragement. He had rehearsals with me before every oral presentation and told me he thinks I will do a great job. I would like to thank Professor Yoshio Nishi at Stanford University for his research advice and providing the samples. I also want to thank the other committee members Professor Zhenqiang Ma and Yu Hen Hu. I am grateful to the department of Electrical and Computer Engineering, especially professor Paul Milenkovic for selecting me as a teaching assistant for 4 years and providing financial assistance to allow me to pursue my degree. I would like to thank professor David Anderson for coming to my commencement.

Many thanks to my colleagues Dongfei, Weiyi, Huifeng, Xiangyu, Faraz, Dan, Kaiwen, Josh, Yuting, Sang-Heum, Haoyu and Yu for their help on the research. They gave me many great suggestions and ideals. I would like to thank all the friends I met in University of Wisconsin-Madison for their friendship and support. I would like to thank the researchers and staff at the Wisconsin Center for Microelectronic (WCAM), Electrical and Computer Engineering and Materials Science and Engineering departments, Taiwan National Synchrotron Radiation Research

Center for their assistance during some experiments. I am especially grateful to the Semiconductor Research Corporation and NSF for their support of my research.

Finally, I would like to express my heartfelt gratitude to my family. I would not be able to do this without my parents' support, understanding and encouragement. I want to thank my husband Silong Li, for his encouragement, love and caring. He always stands by my side through the many years of challenges to pursue our Ph.D. degrees. His companion makes my life in UW-Madison the most joyful experience. I also want to thank him for being my only audience in the final oral examination. You are my love and my soul.

Table of contents

Chapter I. Introduction

A. Motivation……………………………………..……………………….…………1

B. Hypothesis……………………………………………………..……………………..2

C. Tasks to prove the hypothesis……………………….………..…………………….….2

Chapter II. Background

A. Introduction to Resistive random-access memory……………………..………………5

B. Resistive switching mechanism………………………………………….………………5

C. Endurance and switching failure…………………………………………………………7

D. Review of previous work………………………………………….…………10

Chapter III. Theory- TRIM simulation……………………..……………………………20

Chapter IV. Experimental methods and setup

A. I-V characteristics…………………………………………………….….………..24

B. Endurance…………………………………………………………...…………..25

C. Retention …………………………………….……………………...………..27

D. C-V measurements……………………………………………………………..……..28

E. Electron spin resonance…………………………………………..…….………29

F. X-ray diffraction (XRD) ……….……………………………….………………..30

G. Proton radiation sources ……………………………….……………………31

Chapter V. Experimental results

A. Task One results from IV characteristic measurements ……………..……………34

1. Forming process…………………………………….……………………34

2. Set and reset voltage………………………………………………..……..…35

3. HRS resistance as function of proton energy and fluence……….………39

4. Damage self-recovery at room temperature……………..……………..……43

B. Task five results from measurements on blanket films: The effect of proton radiation on HfO_2 blanket films ……………………………………………………...……47

1. Electron spin resonance measurements ……………….……..……….……48

2. C-V and leakage current measurements…………………….…….……….……49

3. X-Ray diffraction XRD……………….…………………………………..…..….53

C. Tasks two, three, and four results from endurance and retention measurements…......54

1. Endurance…………………….……………………………………………..…….…54

a. Endurance measurements and endurance failure…………..………….……54

b. Endurance as a function of proton energy……………….….……...…58

c. Endurance as a function of proton fluence…………………..…..……….61

d. Endurance as a function of temperature……………………..…..…………63

2. Retention……………………..……………………….…………………….….…69

Chapter VI. Summary and conclusions

A. Comparison of experiment with theory…………………..……………..…….……79

B. Conclusion……………………..…………………………………………...………81

C. Future work……………………..……………………………………..…….….…..89

Chapter I. Introduction

A. Motivation

Resistive random-access memory (RRAM) is a type of non-volatile random-access memory (NVM) that operates by changing the resistance of a solid-state dielectric placed between two electrodes. Several new types of nonvolatile memory (NVM), such as magnetic random-access memory (MRAM), phase-changeable memory (PCM), and resistive random-access memory (RRAM), are thought to be promising candidates for flash memory for the next generation of memory applications.[1] Metal-oxide-based RRAMs are promising candidates for universal memory due to their high speed, low power and simple structure. Many metal oxides have been found to exhibit resistive-switching behavior, such as TiO_2, ZrO_2, AlOx and HfO_2. Among these materials, HfO_2-based RRAMs have drawn much attention and have been extensively studied in the past several years. This is because HfO_2-based RRAMs have shown excellent performance, *i.e.* fast switching speed and high endurance.

An important application of NVM is to serve as a memory device for the aerospace and nuclear industries, which requires the memory to have excellent radiation-hardness properties. Environments that contain a large amount of ionizing radiation create special design challenges for RRAM devices. Cosmic rays are a major radiation-damage source and consist of approximately 90% protons. Therefore, in order for HfO_2-based RRAM to be considered for aerospace and nuclear-related applications, it is important to investigate the effects of proton radiation on HfO_2-based RRAM. RRAM is often operated at high temperatures (around 125°C) in the above

applications because of the harsh environment and Joule-heating effects from currents. Therefore, the stability and reliability of proton irradiated devices at high temperature (~ 125°C) is critical for their proper operation.

B. Hypothesis

The hypothesis of this work is that proton radiation with energies from 10-300keV will generate damage to HfO_2-based RRAM that will affect the RRAM cell's resistive switching, reliability, stability and endurance as a function of proton energy and fluence. We further hypothesize that this damage is generated by radiation-induced atomic displacement.

C. Tasks to prove the hypothesis

Task One: Measure RRAM cells' I-V characteristics after proton irradiation to determine whether the proton irradiated RRAM cells are still working. I-V measurements are used to determine the effect of proton radiation on the RRAM's resistive switching characteristics. These are: the HRS and LRS resistances, the forming process, and the set and reset voltages. These will be measured as function of proton energy and proton fluence. In order to find out whether the damage can be recovered, the HRS and LRS resistance of proton irradiated RRAMs will be measured immediately after after irradiation and also after 3 months' storage at room temperature.

Task Two: If the RRAM cells are still working functionally after proton radiation, then reliability tests will be made. In order to determine the effect of proton radiation on the reliability

of RRAM, endurance and retention will be measured. These quantities are key parameters for memory reliability.[1]

Task Three: To measure the stability of the irradiated RRAM cells, the HRS and LRS resistance values (the ratio of HRS resistance to LRS resistance, which is often called the R_{off}/R_{on} ratio) of the proton-irradiated RRAM cells will be measured as a function of the number of switching cycles. This is because switching failures could happen when the R_{on}/R_{off} ratio is too low (< 10).[2]

Task Four: The performance of RRAM is temperature dependent,[3,4] and because proton-induced damage will be enhanced at high temperatures, the resistive switching characteristics, HRS and LRS resistances, and the endurance of proton-irradiated RRAMs will be measured as a function of temperature from room temperature to 150°C, in order to find out how the proton-irradiated RRAM cells behave at high temperature.

Task Five: To determine the cause of the damage, C-V, leakage current, XRD and ESR measurements will be made on HfO_2 blanket films, to be compared with the results of a TRIM simulation. The TRIM simulation will show where displacement damage is predicted. ESR measurements will be made to determine whether displacement damage and oxygen vacancies are generated by the radiation. C-V measurements will be made to determine the radiation-induced defect-charge type and where the defects are generated. If the results of these measurements agree with each other, then it is more likely to prove the hypothesis that the damages are from radiation-induced displacement.

References

[1] Wong, H-S. Philip, Heng-Yuan Lee, Shimeng Yu, Yu-Sheng Chen, Yi Wu, Pang-Shiu Chen, Byoungil Lee, Frederick T. Chen, and Ming-Jinn Tsai. "Metal–oxide RRAM." *Proceedings of the IEEE* 100, no. 6 (2012): 1951-1970.

[2] Chen, Yang Yin, Robin Degraeve, Sergiu Clima, Bogdan Govoreanu, Ludovic Goux, Andrea Fantini, Gouri Sankar Kar et al. "Understanding of the endurance failure in scaled HfO2-based 1T1R RRAM through vacancy mobility degradation." In *Proc. IEEE Electron Devices Meeting* (IEDM), *2012 IEEE International*, pp. 20-3. IEEE, 2012.

[3] Walczyk, Christian, Damian Walczyk, Thomas Schroeder, Thomas Bertaud, Małgorzata Sowinska, Mindaugas Lukosius, Mirko Fraschke et al. "Impact of Temperature on the Resistive Switching Behavior of Embedded HfO2-Based RRAM Devices." *IEEE transactions on electron devices* 58, no. 9 (2011): 3124-3131.

[4] Fang, Z., H. Y. Yu, W. J. Liu, Z. R. Wang, X. A. Tran, B. Gao, and J. F. Kang. "Temperature Instability of Resistive Switching on HfOxBased RRAM Devices." *IEEE Electron Device Letters* 31, no. 5 (2010): 476-478.

Chapter II. Background.

A. Introduction to Resistive random-access memory

RRAM operation involves the generation of defects in a thin-oxide layer, which are typically oxygen vacancies (oxide-bond locations where the oxygen has been removed). The oxygen vacancies can subsequently charge and drift under an electric field.[1] The motion of oxygen ions and vacancies in the oxide is considered to be analogous to the motion of electrons and holes in semiconductors[1].

A RRAM-cell structure is an oxide material sandwiched between two metal electrodes, called a metal-insulator–metal (MIM) structure (Figure 1 (a)). Among such memories, RRAM using binary oxides, like HfO_2, NiO, TiO_2, and ZrO_2, has recently begun to attract attention.[2, 3, 4, 5] RRAM has two states: high-resistance state (HRS) and low-resistance state (LRS). Devices can exhibit resistive switching between these two states. At LRS, oxygen ions migrate from the dielectric, there are more oxygen vacancies in the oxide layer and these generate a path of conductive filaments.

B. Resistive switching mechanism

The switching event from the high-resistance state (HRS) to the low-resistance state (LRS) is called the “set” process. Conversely, the switching event from LRS to HRS is called the “reset process”. Usually, for fresh samples, a voltage higher than the set voltage is needed to initiate the

resistive switching behaviors for subsequent cycles. This initialization is called the "forming" process. Metal-oxide RRAMs have two switching modes: unipolar: the RRAM can switch between the HRS and LRS by using the set and reset voltages that have the same polarity, and bipolar: the RRAM can switch between the HRS and LRS by using set and reset voltages that have opposite polarity.[6] Figure 1 shows a sketch of the IV characteristics of the unipolar (b) and bipolar (c) switching modes.

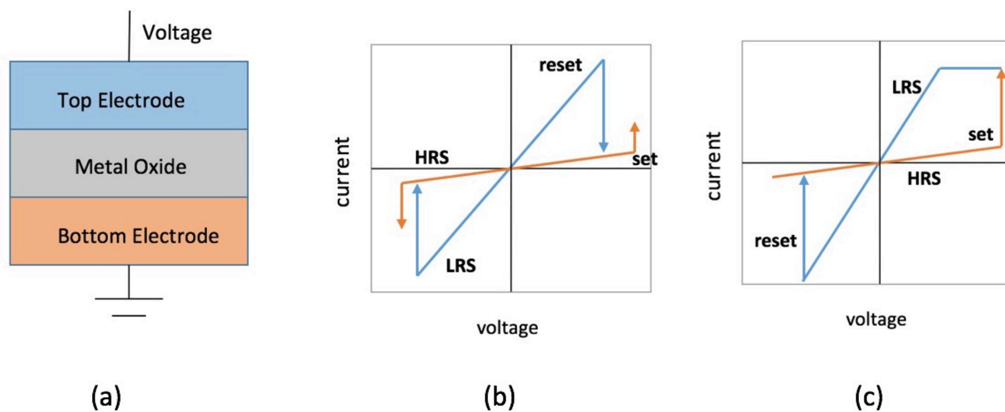

Figure 1. (a) MIM structure of RRAM and IV characteristics of the unipolar (b) and bipolar (c) switching modes.[6]

The forming and set processes for fresh RRAM cells are defined to be a soft dielectric breakdown.[7] Under a relatively high electric field, a soft breakdown occurs and the resistance is significantly reduced. The soft breakdown is recovered when the RRAM cell is reset under a reversed electric field. When a high voltage is applied to the set condition, the deficiency of oxygen leads to the formation of conductive filaments(CFs) that are formed with either oxygen vacancies or metal precipitates.[8] Experimental observations and simulations[9, 10, 11] have previously shown that oxygen migration between the dielectric and the electrodes is present in the switching process and plays an important role in both bipolar and unipolar devices.

Yu et al. [12] proposed a unified reset mechanism for both unipolar and bipolar modes. Figure 2 shows an illustration of the switching processes.[6] During the forming process, soft dielectric breakdown occurs and oxygen ions drift to the anode interface under the influence of the high electric field.[2] The oxygen ions are discharged as neutral non-lattice oxygen during the forming process.[6] For a memory cell in the LRS, the current flows through the conductive filaments (CFs) in the bulk oxide.[13] During the reset process, oxygen ions migrate from the top electrode back to the bulk to recombine with oxygen vacancies that turns the memory cell back into the HRS.[6]

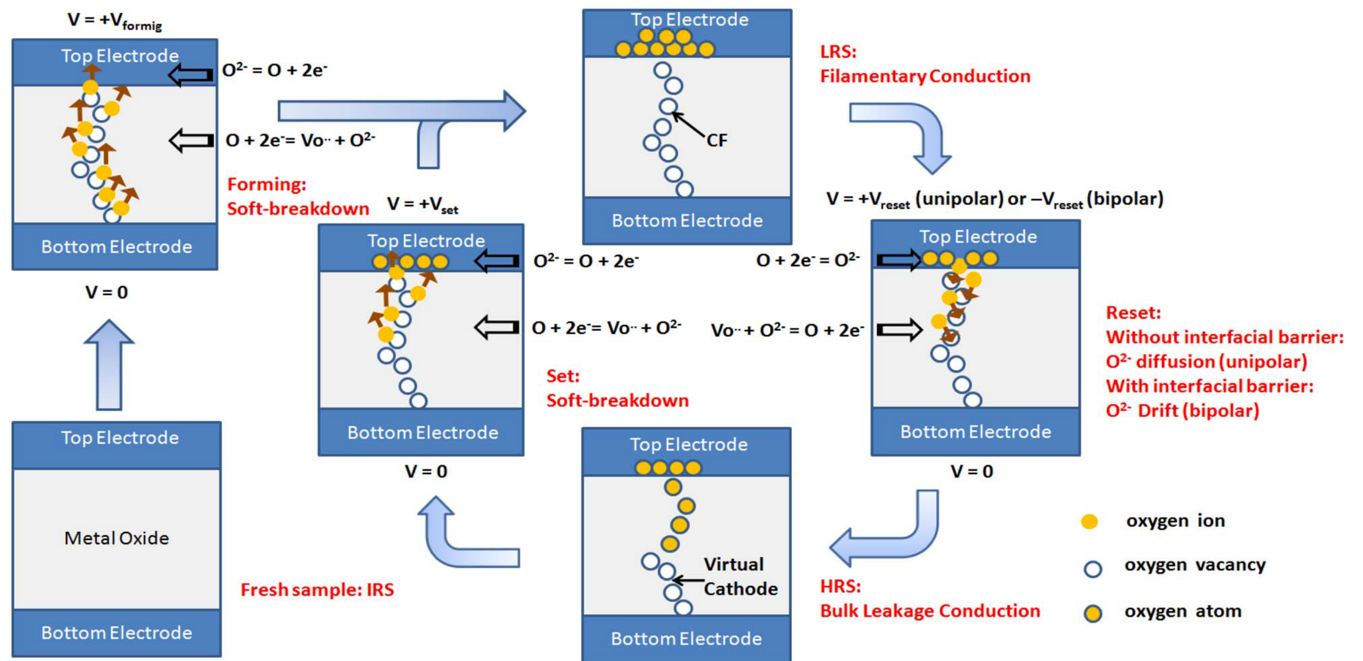

Figure. 2 switching process in the binary metal–oxide RRAM[6]

C. Endurance, retention and switching failure

The endurance of memory is the number of program/erase (P/E cycles) that can be applied to a block of flash memory before the storage media becomes unreliable (when set or reset cannot take place). Cycling or endurance measurement refers to how many operations/cycles the RRAM

cell can sustain, while making sure that the ration R_{HRS}/R_{LRS} is still in the right range (usually 100 to 1000[14]). Cycling of 10^6 is commonly reported.[24] Generally, the endurance of RRAM cells depends on a variety of factors *e.g.*, material, processing, device structure, and operating scheme.[15] Endurance failure can be classified into two modes: set failure and reset failure.[16, 17] It was found that for the low current operation region (LRS $<$ 5kΩ), the dominant endurance failure is SET failure (stuck at HRS), and this endurance failure is depend on the switching frequency. [16] In Reference [18], it was reported that the endurance is related to the SET/RESET pulse amplitude and pulse width. Too high RESET voltage pulses result in the depletion of the oxygen vacancies at the switching interface so that the SET pulse is unable to reconstruct the conducting filaments.[18] In addition, too high SET pulses lead to an excess amount of oxygen vacancies induced at the switching interface so that the RESET pulse is unable to rupture the filaments.[18]

In general, the HRS resistance tends to decrease as the number of switching cycles increases. The final failure state of RRAM cells is the LRS and the cell is unable to reset back to HRS.[19] The resistance change of HRS is gradual at first, then followed by a sharp decrease and finally the RRAM cell remains stuck in LRS.[17] This can be caused by too many defects such as oxygen vacancies that accumulate during the cycling. [21]

Retention refers to how well the cell is capable of retaining the stored information. It reflects the RRAM cells' main nonvolatile property.[24] A RRAM cell should be able to retain stored information for several years. To measure the retention time, the resistances of a RRAM cell are continuously read by using a very small V_{read}. High-temperature retention measurement is usually used to extract activation energies and accelerate the retention testing.[20]

Three different physical mechanisms are proposed to explain the endurance-failure behaviors in reference [21].

1) **Anode-oxidation-induced interface reaction.**

   High temperature, large current and/or power process and oxygen ions produced during the forming and/or SET process can cause oxidation at the electrode interface:

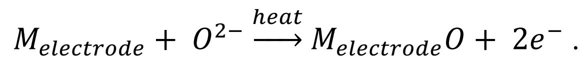

$$M_{electrode} + O^{2-} \xrightarrow{heat} M_{electrode}O + 2e^{-} .$$

2) **Extra vacancies induced.**

   Electric-field-induced extra oxygen vacancies that are generated during switching may increase the conductive filament size.[22] As shown in Figure 3, the increase of the conductive filament (CF) size may cause RESET failure since the rupture of the CFs need more oxygen ions and it therefore becomes more difficult to produce the reset condition.

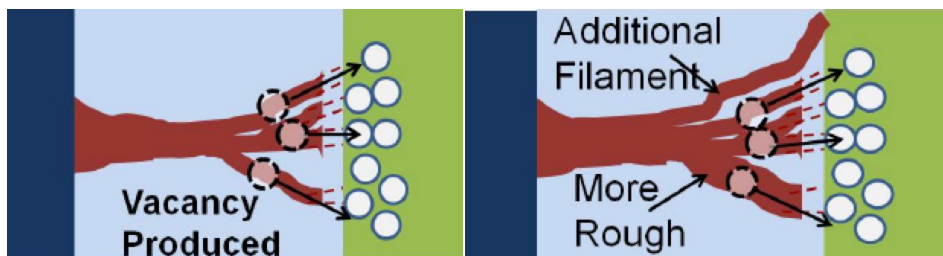

Figure 3. extra vacancy-induced reset failure. Left: oxygen vacancy generated during SET. Right: extra oxygen vacancies generated with more switching cycles. [21]

3) **Depletion of O_2^- induced HRS-resistance reduction.**

   During the RESET process, the oxygen ions recombine with the oxygen vacancies. The drop in oxygen-ion concentration can the reduce the recombination rate of the remaining oxygen vacancies and reduce the HRS resistance.[23] As a result, a higher reset voltage will

be needed to generate more O^{2-}. [21] However, such a reset voltage may cause dielectric breakdown.

D. Review of previous work

Research on RRAM devices has been very active in the last few years. Resistance values of the LRS and HRS states as well as the difference between the LRS and HRS resistances is one of the important quantitates used to characterize RRAM devices. A high R_{HRS}/R_{LRS} ratio enables good differentiation between the information stored in the cell and makes it easier to process. The resistance values of HRA and LRS are also important for designing the memory array and for power consumption issues and to minimize leakage currents through the memory array.[24] Endurance is also an important characteristic of RRAM devices operation. An endurance cycling characterization is the HRS and LRS resistance plotted as a function of the corresponding cycle. This plot allows one to visualize the distribution of resistance values for given operation conductions (same SET and RESET voltage). Usually, the R_{HRS}/R_{LRS} ratio is larger than 100 and there is no overlap of the two HRS and LRS state, which indicates a proper switching operation.[24] In addition to set and reset voltage, retention is also an important characteristic of RRAM.

In recent years, different types of radiation have been used to examine their effects on RRAM. Previous radiation studies on HfO_2-based RRAMs found that Pt/HfO_2:Cu/Cu devices (HfO_2:Cu copper-doped HfO_2) are radiation-immune to a total ionizing dose (TID) of 350 krad(Si) Co-60γ radiation (1.25Mev, ~$10^{14}cm^{-2}$).[25] The total ionizing dose (TID) effect is due to the creation of electron-hole pairs, ionic species and their subsequent reactions.[24] It was found

that RRAM can sustain a TID level of about 5.2 Mrad (1.25MeV, ~10^{15} cm^{-2}) γ rays without significant change in the functionality or the switching characteristics of the RRAM cells.[26] However, the stability of the conductive filaments was weakened and the HRS resistance slightly decreased. The stability degradation is caused by Hf-O bond breaking which can result in oxygen vacancies and non-lattice oxygen in interstitial sites.[25] One-Mev proton radiation was used in the study of total ionizing dose (TID) effects on TiN/HfO_2/TiN RRAM.[27, 28] In reference 28, an HfO_2-based RRAM device was found to have high total ionizing dose (TID) radiation tolerance, including HRS and LRS resistance, set and reset voltage, up to 5 GRads (Si) (equal to 1.77×10^{15} photons/cm^2). After TID irradiation, the device had >10^5 cycles endurance. In reference 27, it was reported that the proton TID radiation *improves* the overall uniformity (less variation on R_{on} and R_{off}) of resistive switching of TiN/HfO_2/TiN Valence change memory RRAM devices. This was explained by the creation of conducting paths between filaments and electrodes due to radiation-induced amorphization. The conducting pathways would serve to reduce cycle-to cycle variation and variations from one device to another.[27]

In another study, energetic ions including 1.6 MeV Ne, 1 MeV He, and 2.75 MeV Ar ions, with fluences ranging from 10^{12} to 10^{15} cm^{-2} were used.[29] The Ar-ion irradiation, which produced the highest displacement damage due to its high mass, was shown to switch some devices from HRS to LRS.[29] It also showed that the degradation of HRS resistance caused by displacement damage is likely to be recovered after several set/reset cycles since the movement of oxygen vacancies and interstitials could create more opportunities for vacancy-interstitial recombination. The same results were seen in this work.

Neutron and proton radiation have been used in the study of displacement damage in $Pt/TiO_2/Pt$ RRAM devices.[30] In reference 30, the $Pt/TiO_2/Pt$ based RRAM cells had no significant changes in their I-V characteristics after 3×10^{14} 1-MeV equivalent neutrons/cm^2 (neutrons with energy from 1-10 MeV). Furthermore, after 7.75×10^{16} 350-keV protons/cm^2 exposure, the off state (HRS) of the device showed a decrease in resistance. This may be explained by the difference in the oxygen vacancies' distribution between the HRS and LRS states. In the HRS state, there is a region in the dielectric film that has very few oxygen vacancies (the gap of the conductive filaments), so that the oxygen vacancies generated by displacement damage in this region could increase the HRS current significantly. Displacement damages to TiO_2 and TaOx-based RRAM cells caused by both 800-keV Ta ions and 28-MeV Si ions caused the HRS resistance to degrade as the oxygen-vacancy concentration increased.[31]

Experiments on TiO_2-based RRAM reported that Co-60 Gamma rays and 941 MeV Bi-ions had only minor effects on resistance values (both HRS and LRS) .[32] The samples could remain in the off state (HRS) and the resistance only changed slightly after both 45 MRad of 1-MeV Co-60 Gamma rays and 23 MRad of 941 MeV Bi-ions irradiation ($\sim10^{15}$ cm^{-2}). Both gamma rays and Bi-ions cause predominantly TID damage in these TiO_2-based RRAM cells. Therefore, these results show that ionization damage, which results in the generation of electron-hole pairs, is unlikely to have a strong effect on the resistive switching of RRAM devices, [24, 28, 30, 31, 32, 33] since the switching mechanism of RRAM is based on the movement of oxygen vacancies.[34] However, displacement damage, which results in the generation of oxygen vacancies and oxygen atoms[35] is likely to have a strong effect on RRAM devices.

References

[1] Sawa, Akihito. "Resistive switching in transition metal oxides." *Materials today* 11.6 (2008): 28-36.

[2] Chen, C., C. Song, J. Yang, F. Zeng, and F. Pan. "Oxygen migration induced resistive switching effect and its thermal stability in W/TaO x/Pt structure." *Applied Physics Letters* 100, no. 25 (2012): 253509.

[3] Wang, Sheng-Yu, Dai-Ying Lee, Tai-Yuen Huang, Jia-Woei Wu, and Tseung-Yuen Tseng. "Controllable oxygen vacancies to enhance resistive switching performance in a ZrO2-based RRAM with embedded Mo layer." *Nanotechnology* 21, no. 49 (2010): 495201.

[4] Jung, Kyooho, Hongwoo Seo, Yongmin Kim, Hyunsik Im, JinPyo Hong, Jae-Wan Park, and Jeon-Kook Lee. "Temperature dependence of high-and low-resistance bistable states in polycrystalline NiO films." *Applied physics letters* 90, no. 5 (2007): 052104.

[5] Long, Shibing, Luca Perniola, Carlo Cagli, Julien Buckley, Xiaojuan Lian, Enrique Miranda, Feng Pan, Ming Liu, and Jordi Suñé. "Voltage and power-controlled regimes in the progressive unipolar RESET transition of HfO2-based RRAM." *Scientific reports* 3 (2013).

[6] Wong, H-S. Philip, Heng-Yuan Lee, Shimeng Yu, Yu-Sheng Chen, Yi Wu, Pang-Shiu Chen, Byoungil Lee, Frederick T. Chen, and Ming-Jinn Tsai. "Metal–oxide RRAM." *Proceedings of the IEEE* 100, no. 6 (2012): 1951-1970.

---

[7] Xu, Nuo, Lifeng Liu, Xiao Sun, Xiaoyan Liu, Dedong Han, Yi Wang, Ruqi Han, Jinfeng Kang, and Bin Yu. "Characteristics and mechanism of conduction/set process in TiN⁄ ZnO⁄ Pt resistance switching random-access memories." *Applied Physics Letters* 92, no. 23 (2008): 232112.

[8] Kim, Kyung Min, Byung Joon Choi, and Cheol Seong Hwang. "Localized switching mechanism in resistive switching of atomic-layer-deposited Ti O 2 thin films." *Applied physics letters* 90.24 (2007): 242906.

[9] Yoshida, Chikako, Kentaro Kinoshita, Takahiro Yamasaki, and Yoshihiro Sugiyama. "Direct observation of oxygen movement during resistance switching in NiO/Pt film." Applied Physics Letters 93, no. 4 (2008): 042106.

[10] Yu, Shimeng, Ximeng Guan, and H-S. Philip Wong. "Understanding metal oxide RRAM current overshoot and reliability using kinetic Monte Carlo simulation." *In Electron Devices Meeting (IEDM)*, 2012 IEEE International, pp. 26-1. IEEE, 2012.

[11] Kumar, Suhas, Ziwen Wang, Xiaopeng Huang, Niru Kumari, Noraica Davila, John Paul Strachan, David Vine, AL David Kilcoyne, Yoshio Nishi, and R. Stanley Williams. "Oxygen migration during resistance switching and failure of hafnium oxide memristors." *Applied Physics Letters* 110, no. 10 (2017): 103503.

[12] Yu, Shimeng, and H-S. Philip Wong. "A phenomenological model for the reset mechanism of metal oxide RRAM." *IEEE Electron Device Letters* 31, no. 12 (2010): 1455-1457.

[13] Kumar, Suhas, Ziwen Wang, Xiaopeng Huang, Niru Kumari, Noraica Davila, John Paul Strachan, David Vine, AL David Kilcoyne, Yoshio Nishi, and R. Stanley Williams. "Oxygen migration during resistance switching and failure of hafnium oxide memristors." *Applied Physics Letters* 110, no. 10 (2017): 103503.

[14] Jo, S. H. "Recent progress in rram materials and devices." SEMICON Korea 138 (2015).

[15] Cheng, C. H., C. Y. Tsai, Albert Chin, and F. S. Yeh. "High performance ultra-low energy RRAM with good retention and endurance." *In Electron Devices Meeting (IEDM)*, 2010 IEEE International, pp. 19-4. IEEE, 2010.

[16] Chen, Yang Yin, Robin Degraeve, Sergiu Clima, Bogdan Govoreanu, Ludovic Goux, Andrea Fantini, Gouri Sankar Kar et al. "Understanding of the endurance failure in scaled HfO 2-based 1T1R RRAM through vacancy mobility degradation." *In Electron Devices Meeting (IEDM)*, 2012 IEEE International, pp. 20-3. IEEE, 2012.

[17] Huang, P., B. Chen, Y. J. Wang, F. F. Zhang, L. Shen, R. Liu, L. Zeng et al. "Analytic model of endurance degradation and its practical applications for operation scheme optimization in metal oxide based RRAM." *In Electron Devices Meeting (IEDM)*, 2013 IEEE International, pp. 22-5. IEEE, 2013.

---

[18] Chen, Yang Yin, Bogdan Govoreanu, Ludovic Goux, Robin Degraeve, Andrea Fantini, Gouri Sankar Kar, Dirk J. Wouters et al. "Balancing SET/RESET Pulse for > 10 10Endurance in HfO2/Hf 1T1R Bipolar RRAM." *IEEE Transactions on Electron devices* 59, no. 12 (2012): 3243-3249.

[19] Wong, H-S. Philip, Heng-Yuan Lee, Shimeng Yu, Yu-Sheng Chen, Yi Wu, Pang-Shiu Chen, Byoungil Lee, Frederick T. Chen, and Ming-Jinn Tsai. "Metal–oxide RRAM." *Proc. IEEE* 100, no. 6 (2012): 1951-1970.

[20] Jameson, J. R., P. Blanchard, C. Cheng, J. Dinh, A. Gallo, V. Gopalakrishnan, C. Gopalan et al. "Conductive-bridge memory (CBRAM) with excellent high-temperature retention." In *Proc. IEEE Electron Devices Meeting* (IEDM), 2013 *IEEE International*, pp. 30-1. IEEE, 2013.

[21] Chen, B., Y. Lu, B. Gao, Y. H. Fu, F. F. Zhang, P. Huang, Y. S. Chen et al. "Physical mechanisms of endurance degradation in TMO-RRAM." In *Proc. IEEE Electron Devices Meeting* (IEDM), 2011 IEEE International, pp. 12-3. IEEE, 2011.

[22] Huang, P., B. Chen, Y. J. Wang, F. F. Zhang, L. Shen, R. Liu, L. Zeng et al. "Analytic model of endurance degradation and its practical applications for operation scheme optimization in metal oxide based RRAM." In *Proc. IEEE Electron Devices Meeting* (IEDM), 2013 IEEE International, pp. 22-5. IEEE, 2013.

[23] Gao, B., S. Yu, N. Xu, L. F. Liu, B. Sun, X. Y. Liu, R. Q. Han, J. F. Kang, B. Yu, and Y. Y. Wang. "Oxide-based RRAM switching mechanism: A new ion-transport-recombination model." In *Electron Devices Meeting*, 2008. IEDM 2008. IEEE International, pp. 1-4. IEEE, 2008.

[24] Gonzalez-Velo, Yago, Hugh J. Barnaby, and Michael N. Kozicki. "Review of radiation effects on ReRAM devices and technology." *Semiconductor Science and Technology* 32, no. 8 (2017): 083002.

[25] Wang, Yan, Hangbing Lv, Wei Wang, Qi Liu, Shibing Long, Qin Wang, Zongliang Huo et al. "Highly stable radiation-hardened resistive-switching memory." *IEEE Electron Device Letters* 31, no. 12 (2010): 1470-1472.

[26] Fang, Runchen, Yago Gonzalez Velo, Wenhao Chen, Keith E. Holbert, Michael N. Kozicki, Hugh Barnaby, and Shimeng Yu. "Total ionizing dose effect of γ-ray radiation on the switching characteristics and filament stability of HfOx resistive random access memory." *Applied Physics Letters* 104, no. 18 (2014): 183507.

[27] He, Xiaoli, Wei Wang, Brian Butcher, Sansiri Tanachutiwat, and Robert E. Geer. "Superior TID hardness in TiN/HfO2/TiN ReRAMs after proton radiation." *IEEE Trans. Nucl. Sci* 59, no. 5 (2012): 2550-2555.

[28] He, Xiaoli, and Robert E. Geer. "High Total-Dose Proton Radiation Tolerance in TiN/HfO 2/TiN ReRAM Devices." *MRS Online Proceedings Library* Archive 1430 (2012).

---

[29] He, Xiaoli, and Robert E. Geer. "Heavy ion radiation effects on TiN/HfO 2/W resistive random access memory." *In Aerospace Conference*, 2013 IEEE, pp. 1-7. IEEE, 2013.

[30] DeIonno, E., M. D. Looper, J. V. Osborn, and J. W. Palko. "Displacement Damage in TiO2 Memristor Devices." *IEEE Transactions on Nuclear Science* 60, no. 2 (2013): 1379-1383.

[31] Hughart, David R., Andrew J. Lohn, Patrick R. Mickel, Scott M. Dalton, Paul E. Dodd, Marty R. Shaneyfelt, Antoinette I. Silva et al. "A Comparison of the Radiation Response of TaOx and TiO2 Memristors." *IEEE Trans. Nucl. Sci* 60, no. 6 (2013): 4512-4519.

[32] Tong, William M., J. Joshua Yang, Philip J. Kuekes, Duncan R. Stewart, R. Stanley Williams, Erica DeIonno, Everett E. King, Steven C. Witczak, Mark D. Looper, and Jon V. Osborn. "Radiation Hardness of TiO_2 Memristive Junctions." *IEEE Trans. Nucl. Sci* 57, no. 3 (2010): 1640-1643.

[33] Zhang, Lijie, Ru Huang, Dejin Gao, Pan Yue, Poren Tang, Fei Tan, Yimao Cai, and Yangyuan Wang. "Total Ionizing Dose (TID) Effects on TaOx-Based Resistance Change Memory." *IEEE Trans. on Electron Devices* 58, no. 8 (2011): 2800-2804.

---

34 Holt, Joshua S., Karsten Beckmann, Zahiruddin Alamgir, Jean Yang-Scharlotta, and Nathaniel C. Cady. "Effect of Displacement Damage on Tantalum Oxide Resistive Memory." *MRS Advances* 2, no. 52 (2017): 3011-3017.

[35] Srour, J. R., Cheryl J. Marshall, and Paul W. Marshall. "Review of displacement damage effects in silicon devices." *IEEE Trans. Nucl. Sci* 50, no. 3 (2003): 653-670.

Chapter III. Theory-TRIM simulation.

The Stopping and Range of Ions in Matter (SRIM) or Transport of Ions in Matter (TRIM) codes[1] are popular in the ion-implantation research and technology community and also used widely in other branches of materials science. The TRIM code is based on a Monte-Carlo simulation. As output, it lists or plots the distribution of the ions in a solid and its parameters, such as penetration depth, concentration of vacancies, sputtering rate, ionization, and phonon production in the target material. [2]

The SRIM-2008 (Stopping and Range of Ions in Matter) package was downloaded online. As input parameters, it needs the ion type and energy (in range 10 eV to 2 GeV) and a target material of one or several layers. In the simulation, H ions were implanted. In order to make the simulation conditions closer to those of a RRAM cell, the target material has three layers. Si substrate, 5-nm HfO_2 and 40-nm TiN. The angel of implanted ions is 5 degrees with respect to the vertical direction of the film surface. Five thousand ions were implanted in each simulation run.

Figure 1 presents the TRIM results for three ion energies, showing the distribution of the protons throughout the oxide after irradiation. For the low-energy exposure, more protons are seen to stay in the HfO_2 film, however, 300keV protons have enough energy so that most of them pass through the HfO_2 film. The results of 100keV case are in between as shown in the Figure below. As output, the simulation software can plot the distribution of the ions in the target material. It can also show the damage events, such as location of vacancies, sputtering rate, and ionization. The results of damage events on the right show that more vacancies are generated in the HfO_2 film

during lower proton energy irradiation. In chapter V, the HRS resistance and endurance measurements results show the proton radiation induced oxygen vacancies could be recovered during reset process. High energy proton radiation generate more long lasting defects and those defects affect the HRS resistance and endurance.

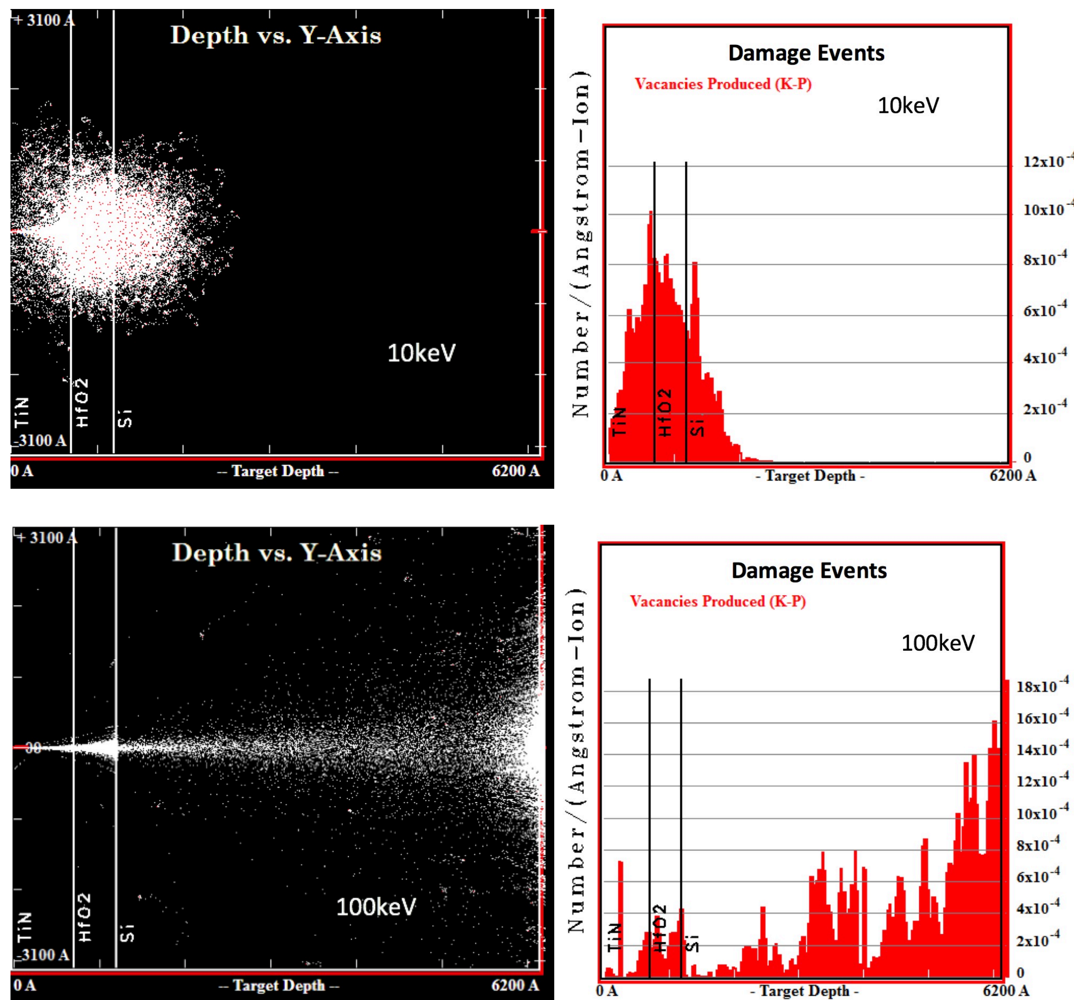

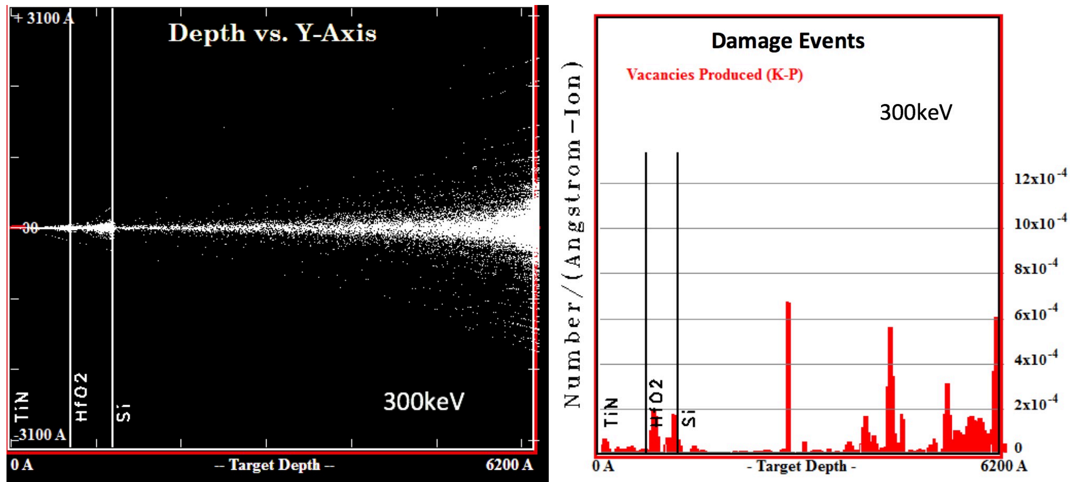

Figure 1. The 10, 100 and 300-keV H-ion implantation damage from TRIM simulation The results on the right show where the collision/displacement event happens and the distribution of vacancies generated from displacement damage.

References

[1] https://en.wikipedia.org/wiki/Stopping_and_Range_of_Ions_in_Matter

[2] Biersack, Jochen P., and L. G. Haggmark. "A Monte Carlo computer program for the transport of energetic ions in amorphous targets." *Nuclear Instruments and Methods* 174, no. 1-2 (1980): 257-269.

Chapter IV. Experimental methods and setup

In this work, the RRAM devices used are fabricated with a Pt/HfO_2/TiN metal-insulator-metal structure, as shown in Figure 1. The 5-nm thick HfO_2 films were deposited by atomic layer deposition. The RRAM cells were made in Stanford University. The bottom and top electrodes are Pt and TiN, respectively. The proton irradiation was performed using H-ion implantation. Ten, 100 and 300-keV energies were chosen based on the TRIM simulation. In addition, five different proton-radiation fluences were used: 10^9, 10^{11}, 10^{13}, 10^{14}, and 10^{15} photons/cm^{-2}. The maximum fluence was picked based on the total ionizing dose (TID) level that HfO_2-based memory can sustain[1] .

A. I-V characteristics

The I-V characteristics of RRAM were measured using a HP 4155B semiconductor-parameter analyzer. A probe station with an optical microscope was used to make contact with the RRAM cell. The current was measured with two probes placed in contact with the two electrodes of a RRAM cell. The structure of the HfO_2 RRAM cell used in this work is shown on the left in Figure 1. Pt is used as the bottom electrode and the top electrode is TiN. This RRAM cell has a bipolar switching mode, which means the switching direction depends on the polarity of applied voltage. Then the set and reset voltage were read from the I-V curve and the resistance were calculated based on the I-V curve.

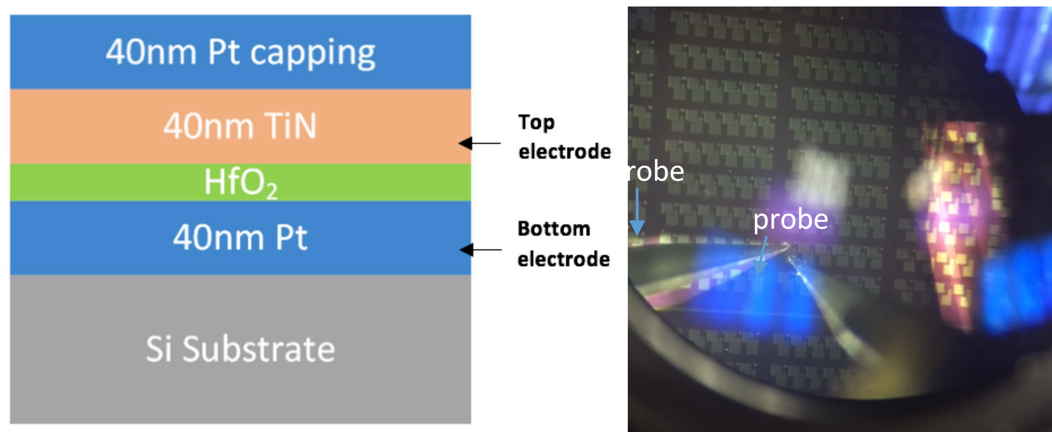

Figure 1. left: structure of RRAM cell and right: optical micrograph of RRAM top structure during I-V measurement.

B. Endurance

The long-term reliability of proton-irradiated RRAM plays a critical role in determining the viability of HfO_2-based RRAM for use in space applications.[2] Endurance is one of the essential criteria for any memory application. A circuit diagram for the endurance measurements is shown in Figure 2 (a) and (b). The pulse signal used is shown in Figure 2 (c). The signal amplitude is picked based the measured set and reset voltage. The frequency of the signal is 100kHz. This signal will make sure the RRAM cells have enough voltage and wait time to switch. The I-V characteristics were measured with an HP 4155B Semiconductor-parameter analyzer. The voltages were applied to the top electrode and the bottom electrode was grounded during the measurements. Approximately 20-30 RRAM cells were measured in each case to get the endurance statistics.

Limiting the current during the set process could control the size of conductive filament and the LRS current after set, whereas the stop voltage during reset process effect the HRS.[3] Current

compliance is a parameter that can be set in the HP 4155B to protect the device from breaking down at LRS. It is the highest current that can flow through the device during the I-V measurements. Start voltage and stop voltage are others parameters that can be set. The voltage sweep will start from start voltage and stop when it get to the stop voltage. Thus, in all the endurance measurements, the current compliance and stop voltage are held constant. For room-temperature measurements, the current compliance was 30μA and the stop voltage was -2.7V, and for high temperature, the current compliance was 50μA and the stop voltage was -2.6V. The swept voltage during reset is from 0V to the stop voltage. The current during measurements will not exceed than the current compliance.

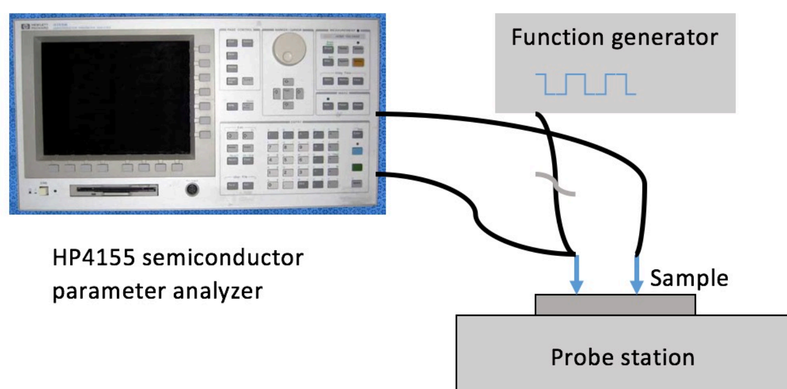

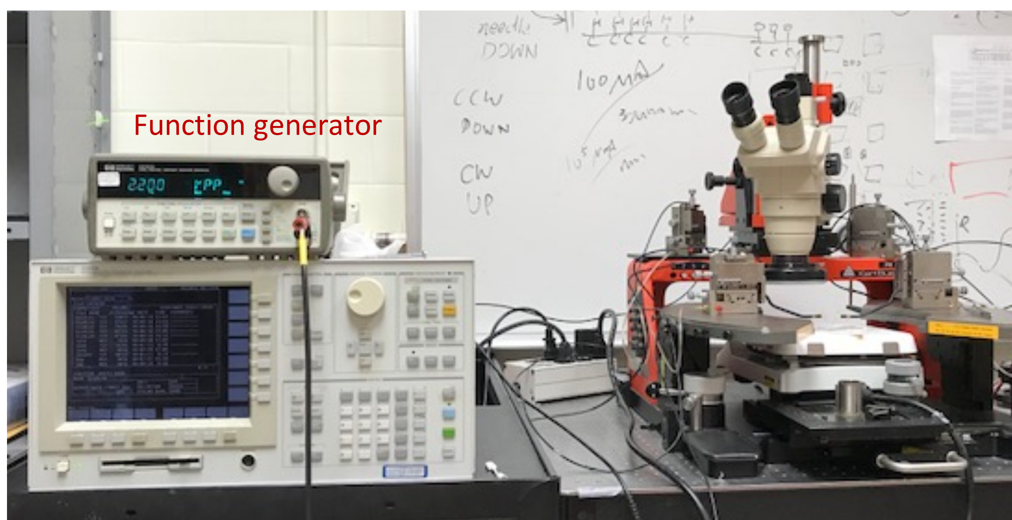

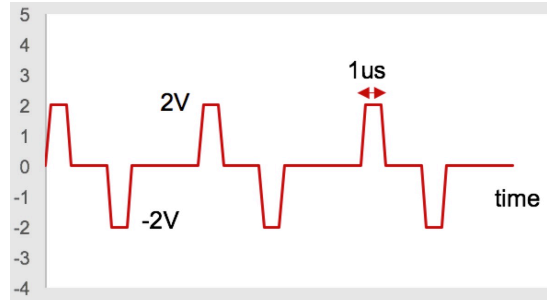

Figure 2. (a). circuit diagram and (b). the actual setup for the endurance measurement, (c). pulse signal for endurance.

C. Retention

A data retention time longer than ten years is expected for nonvolatile memory. The retention must be maintained at its operating temperature. To measure this, a small electrical stress (such as read voltage) is applied.[4] The retention time was measured by using a HP 4155B semiconductor parameter analyzer, a probe station and a hot plate. Labview was used to control the semiconductor-parameter analyzer. The devices are heated to 120°C with a hot plate, The HRS and LRS resistances are monitored by applying read voltage (0.5V) pulses every 10 seconds. In actual operation, the read voltage is smaller than 0.3V.[5] However, in order to speed up the dielectric breakdown, a higher temperature and higher read voltage has been used. The I-V characteristics were measured before and after the retention measurement to make sure the RRAM devices did not fail during the retention measurement. The extrapolation to room temperature will be explained in the results section.

Measurements on HfO2 blanket films:

In order to determine the cause of the damage, C-V, XRD and ESR measurements will be made on HfO_2 blanket films, to be compared with the results of TRIM simulation. Two different thickness of HfO_2 film were used: 5 and 100 nm. The 5-nm blanket films are same as the 5-nm HfO_2 layer in RRAM and thus, 5-nm blanket film were used in most of the following measurements. However, 5-nm is too thin for XRD measurements. One-hundred nm blanket film was therefore also used for XRD measurements, as well as CV and leakage current measurements. Both films were made by ALD, they are deposited in the same way as the HfO_2 film in RRAM.

D. C-V measurements

The C-V characteristics of HfO_2 blanket film were measured using a HP 4285A LCR Precision meter at high frequency (1MHz). A probe station with an optical microscope was used to make contact with the samples. Metal electrodes were deposited on the top of the HfO_2 film with vacuum evaporation so that the samples for C-V measurement have a MOS structure. The metal electrode has a structure of 200-nm silver on top of 30-nm titanium.

E. Electron spin resonance

Electron spin resonance (ESR) spectroscopy is a very powerful and sensitive method for the characterization of the electronic structures of materials with unpaired electrons. An electron-spin resonance experiment generally consists of measuring the absorption of microwave power at a fixed frequency as a function of an applied laboratory magnetic field B.[6,] It has been applied to various high-k dielectrics, such as SiO_2 and HfO_2.[7] In this work, the ESR measurements were made with an X-band Bruker Elexsys 500E EPR spectrometer. A 0.0003% KCl weak-pitch sample was used to calibrate the system (10^{13}spins/cm).

To determine the cause of damage, electron-spin-resonance measurements were made on the 5-nm thick ALD HfO_2 blanket films on Si substrate before (pristine) and after proton irradiation. In this work, the ESR measurements were made with an X-band Bruker Elexsys 500E EPR spectrometer.

Each defect has its fingerprint, *i.e.*, the g-factor, which depends on the microwave frequency and the magnetic field strength as:[6, 8]

$$g = \frac{hv}{\mu_B B_0} \quad (1)$$

where h is Planck's constant, μ_B is the Bohr magnetron $\frac{eh}{4\pi m_e}$, v is the frequency of the oscillating magnetic field and B_0 is the magnetic field strength at the peak of ESR absorption for each defect. Experimentally, the absorption spectral signals are written as a Lorentzian derivative. The integral of the Lorentzian distribution is used to determine the concentration of the defects. They can be easily expressed as:

$$f'_{Lorentz}(B) = -\frac{\frac{2A(B-B_0)}{\sigma}}{[1+(\frac{(B-B_0)}{\sigma})^2]^2} \quad (3)$$

and

$$C_{Lorentz} = \int_{B_{low}}^{B_{high}} f_{Lorentz}(B)dB \propto \sqrt{\pi}A\sigma \quad (3)$$

where $f'_{Lorentz}(B)$ is the signal shape of Lorentzian derivative and $C_{Lorentz}$ represents the concentration of the defect state.[7] B_{high} and B_{low} are the maximum and minimum values of the scanned magnetic field. σ is defined as the B-field width that represents the width of the ESR spectroscopic signal and A represents the amplitude of the distribution.[8]

F. X-ray diffraction (XRD)

X-ray diffraction is a destructive analytical technique that reveals information about the crystal structure, chemical composition, and physical properties of materials and thin films. A Bruker D8 Discover diffractometer is used in this work to measure the structure of 100-nm thick HfO_2 films before and after proton irradiation. As mentioned earlier, the 5nm blanket film is too thin for XRD

measurements. The 100nm blanket film were made in the same way as the 5nm samples. The blanket HfO_2 film is polycrystalline (monoclinic). This can be seen from the XRD results.

G. Radiation sources

The protons used in this work were generated by using H-ion implantation. In order to investigate the damage as a function of proton energy and fluence, both blanket HfO_2 films and RRAM cells were exposed to protons with three different energies based on the TRIM simulation results: 10, 100 and 300-keV respectively. In addition, 5 different proton-radiation fluences were used: 10^9, 10^{11}, 10^{13}, 10^{14}, and 10^{15} photons/cm^{-2}. Again, the energies were chosen based on simulation results and the maximum fluence was picked based on the total ionizing dose (TID) level that HfO_2-based memory can sustain.[9] The ion implantation was performed at Luxience Technology.

References

[1] Fang, Runchen, Yago Gonzalez Velo, Wenhao Chen, Keith E. Holbert, Michael N. Kozicki, Hugh Barnaby, and Shimeng Yu. "Total ionizing dose effect of γ-ray radiation on the switching characteristics and filament stability of HfOx resistive random access memory." *Applied Physics Letters* 104, no. 18 (2014): 183507.

[2] Felix, J. A., J. R. Schwank, Daniel M. Fleetwood, M. R. Shaneyfelt, and Evgeni P. Gusev. "Effects of radiation and charge trapping on the reliability of high-κ gate dielectrics." *Microelectronics Reliability* 44, no. 4 (2004): 563-575.

[3] Balatti, Simone, Stefano Ambrogio, Z-Q. Wang, S. Sills, A. Calderoni, N. Ramaswamy, and Daniele Ielmini. "Pulsed cycling operation and endurance failure of metal-oxide resistive (RRAM)." *In Electron Devices Meeting (IEDM)*, 2014 IEEE International, pp. 14-3. IEEE, 2014.

[4] Chen, Yang Yin, Ludovic Goux, Sergiu Clima, Bogdan Govoreanu, Robin Degraeve, Gouri Sankar Kar, Andrea Fantini, Guido Groeseneken, Dirk J. Wouters, and Malgorzata Jurczak. "Endurance/retention trade-off on HfO2/metal cap 1T1R bipolar RRAM." *IEEE Trans Electron Devices* 60 (2013): 1114.

[5] Puglisi, Francesco Maria, Altin Qafa, and Paolo Pavan. "Temperature impact on the reset operation in HfO2 RRAM." *IEEE Electron Device Lett* 36, no. 3 (2015): 244-246.

[6] Griscom, David L. "Electron spin resonance in glasses." *Journal of Non-Crystalline Solids* 40, no. 1-3 (1980): 211-272.

[7] Ren, H., S. L. Cheng, Y. Nishi, and J. L. Shohet. "Effects of vacuum ultraviolet and ultraviolet irradiation on ultrathin hafnium-oxide dielectric layers on (100) Si as measured with electron-spin resonance." Applied Physics Letters 96, no. 19 (2010): 192904.

[8] Griscom, D. L. "Electron spin resonance." In Glass Science and Technology, vol. 4, pp. 151-251. *Elsevier*, 1990.

[9] Wang, Yan, Hangbing Lv, Wei Wang, Qi Liu, Shibing Long, Qin Wang, Zongliang Huo et al. "Highly stable radiation-hardened resistive-switching memory." *IEEE Electron Device Letters* 31, no. 12 (2010): 1470-1472.

Chapter V. Experimental results.

A. Task One results from IV characteristic measurements:

1. Forming process

All of the fresh pristine RRAM cells need to be formed. The forming voltage is approximately 3.4 - 3.7 V. However, a number of low-energy proton-exposed samples were found to have been formed and set after irradiation. For the devices measured within a week after proton irradiation, about 30% of the 10-keV proton-irradiated devices were formed by irradiation and turned to LRS without applying any electric field. However, the 100 and 300-keV proton-exposed RRAM samples were not formed or set after proton exposure. As shown in Figure 1, for those RRAM cells that were not formed under proton radiation, the forming voltages are about the same as those needed in the pristine case. Those RRAM cells that are formed and set to LRS by proton irradiation could be reset to HRS during the reset process when a negative was applied on the top electrode. This radiation-induced forming process could be explained as radiation-induced dielectric soft breakdown.[1, 2]

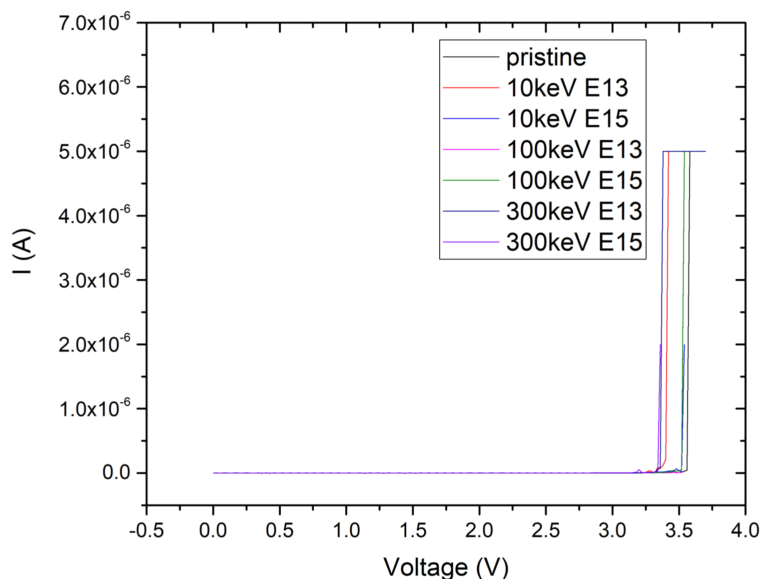

Figure 1. The forming process of fresh RRAM cells. All of the pristine RRAM cells need to be formed.

The fact that 10-keV proton-irradiated samples were formed and set to LRS is likely caused by oxygen displacement damage and broken O-Hf bonds.[3, 4] The oxygen vacancies and oxygen ions/oxygen atoms are generated during proton irradiation. When the fluences are the same, there are more oxygen vacancies generated in the 10-keV proton irradiated samples than the 300-keV samples during the proton radiation. Therefore, the oxygen vacancies created in the HfO_2 can act as a conductive filament and turn the RRAM to LRS. [5, 6] Then, during the reset process, the oxygen ions migrate back into to the HfO_2 film and thus most of the proton-induced oxygen vacancies near the electrode are recombined with the oxygen ions, so that the RRAM cells can be reset to HRS state.

2. Set and reset voltage

Except for the fact that some of the 10keV RRAM cells are formed by the proton radiation, these proton-irradiated RRAM devices work functionally. Figure 2 shows a typical pristine

resistive-switching I-V characteristic of several cycles in one fresh device which need a forming process. To reset the device from LRS to HRS, a negative voltage sweeps from 0 to -2.8V is used, to set the device from HRS to LRS, a positive voltage sweep from 0 to 2.5V is used with a current compliance of 50 to 10 μA.

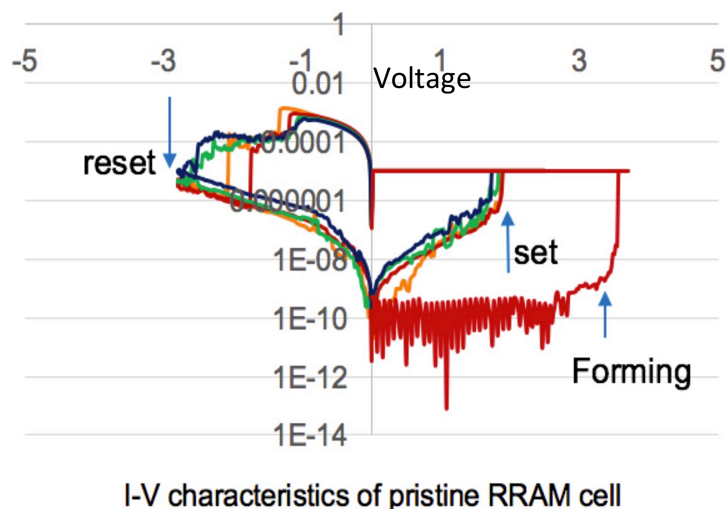

Figure 2. I-V characteristics of pristine RRAM cell

The set and reset voltage amplitude distributions were examined after irradiation. As shown in Figures 3 and 4, the average amplitudes of set and reset voltage did not significantly decrease after 10 to 300keV proton irradiation. The average values showed in the Figure 4 are listed in Table 1.

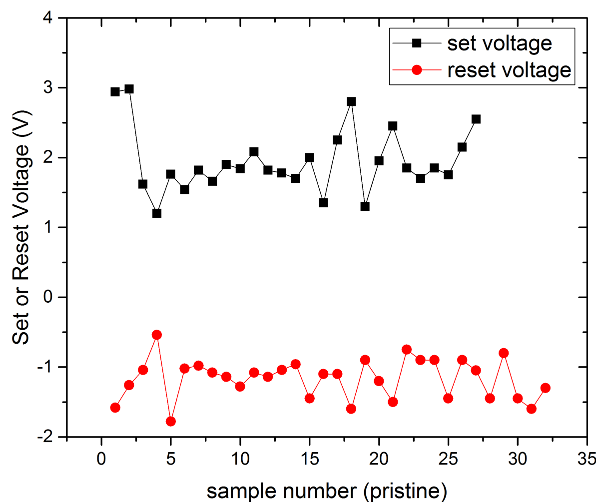

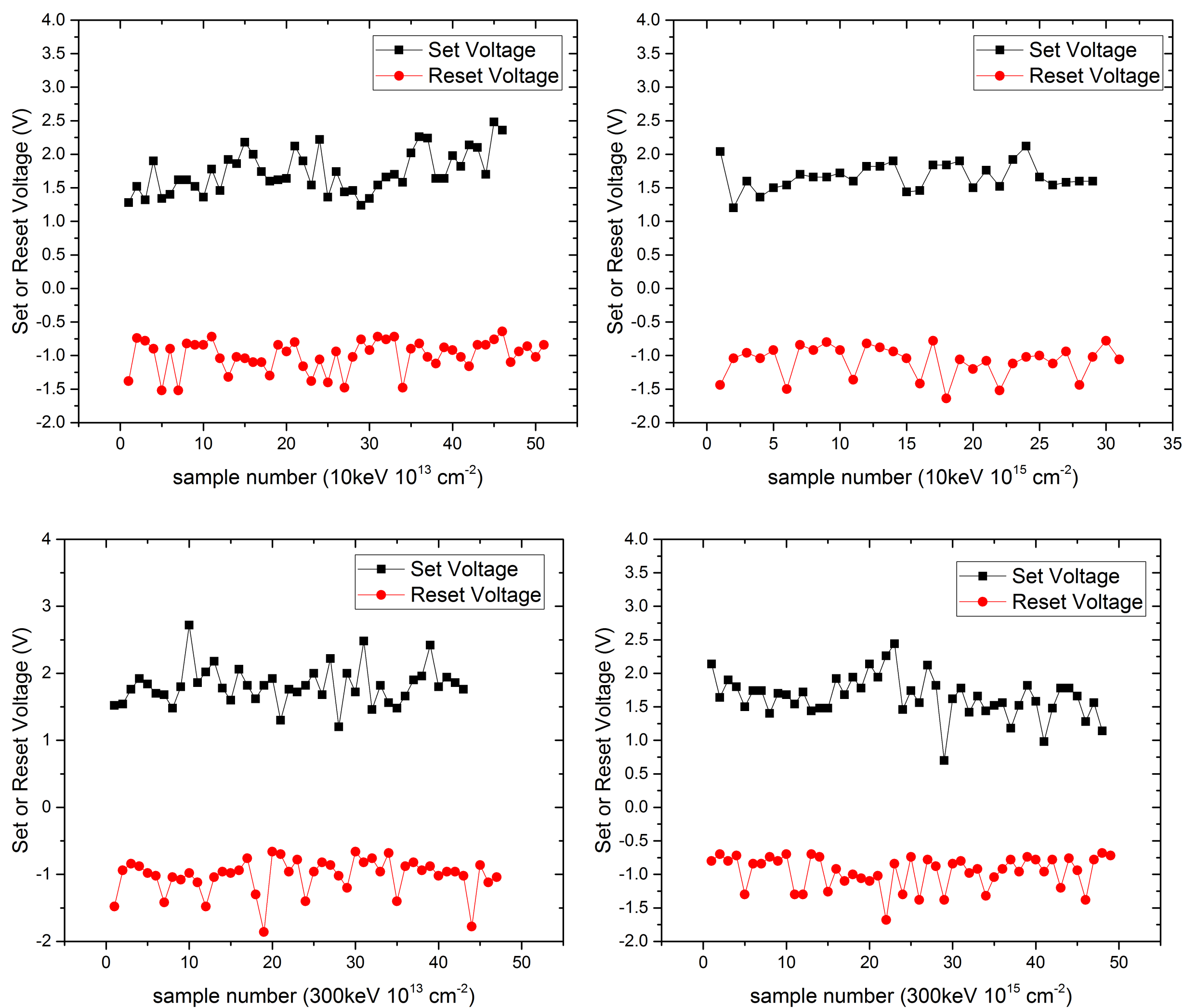

Figure 3. the set and reset voltage of each sample after irradiation The values in each figure are not in any specific order.

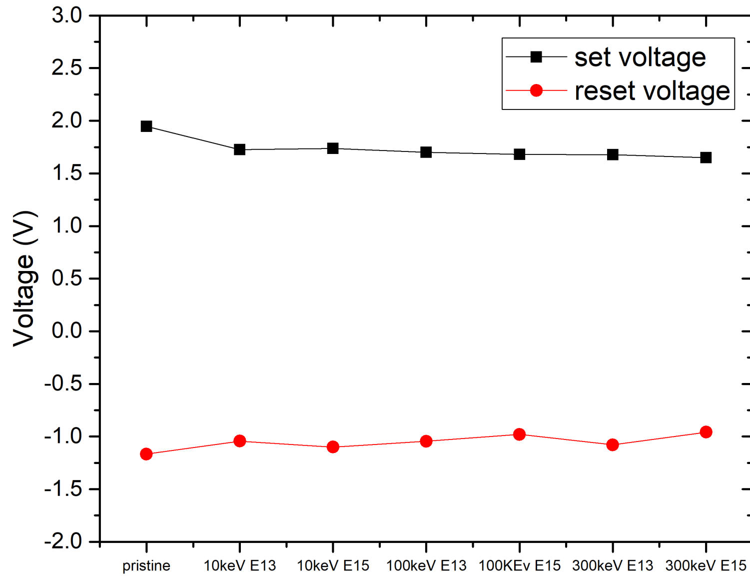

Figure 4. Average values of set and reset voltage of pristine and proton-irradiated RRAM for a range of fluences and energies.

	Set (V)	**Variance**	**Reset (V)**	**Variance**
pristine	1.948±0.7	0.12	-1.166±0.3	0.08
10keV $10^{13}cm^{-2}$	1.726±0.7	0.03	-1.043±0.4	0.06
10keV $10^{15}cm^{-2}$	1.737±0.5	0.08	-1.122±0.3	0.04
100keV $10^{13}cm^{-2}$	1.7±0.5	0.08	-1.045±0.4	0.05
100keV $10^{15}cm^{-2}$	1.68±0.4	0.04	-0.98±0.4	0.07
300keV $10^{13}cm^{-2}$	1.677±0.7	0.04	-1.0796±0.6	0.06
300keV $10^{15}cm^{-2}$	1.649±0.8	0.09	-0.959±0.4	0.06

Table 1. The average values of set and reset voltage.

3. HRS resistance as function of proton energy and fluence

Next, the HRS resistances of pristine and proton-irradiated RRAM cells are calculated based on the IV-characteristics. The average resistance values of each case are calculated based on more than 50 data points. Since those samples that are formed by radiation could be reset and still work functionally, the formed and non-formed RRAM cells are not separated here.

The results show that the HRS resistance decreased after proton radiation. Figure 5 shows the I-V characteristics of pristine and proton irradiated RRAM cells measured within a week after proton irradiation. In Figure 5 a), the 300-keV proton-irradiated samples show more significant differences before and after proton irradiation, while the 10-keV proton-irradiated case shows a smaller difference. The HRS resistance of the 300-keV irradiated samples measured at -0.5V is about 17-19 times smaller compared with the pristine samples. The HRS resistance of the 10-keV irradiated samples is 7-10 times smaller than that for the pristine samples. This bias was chosen because -0.5V is lower than the reset voltage, so at -0.5V, the LRS and HRS resistances are significantly different. This decrease of resistance occurs, as has we have shown, after proton irradiation which causes displacement damage that generates oxygen vacancies in the HfO_2. There are a lot of oxygen vacancies (conductive filaments) in LRS to make the resistance very low, so that the proton-induced oxygen vacancies have little effect on the LRS resistance. Figure 5 b) shows the first 3 reset cycles of a 300keV $10^{13}cm^{-2}$ proton irradiated RRAM cell. It shows that both HRS and LRS currents are getting lower with each reset cycle. This further shows that after proton radiation, some of the radiation-induced oxygen vacancies are recombined with oxygen ion

during the reset process. The decreasing of LRS and HRS currents (increasing LRS and HRS resistance) means there are less oxygen vacancies with more reset process.

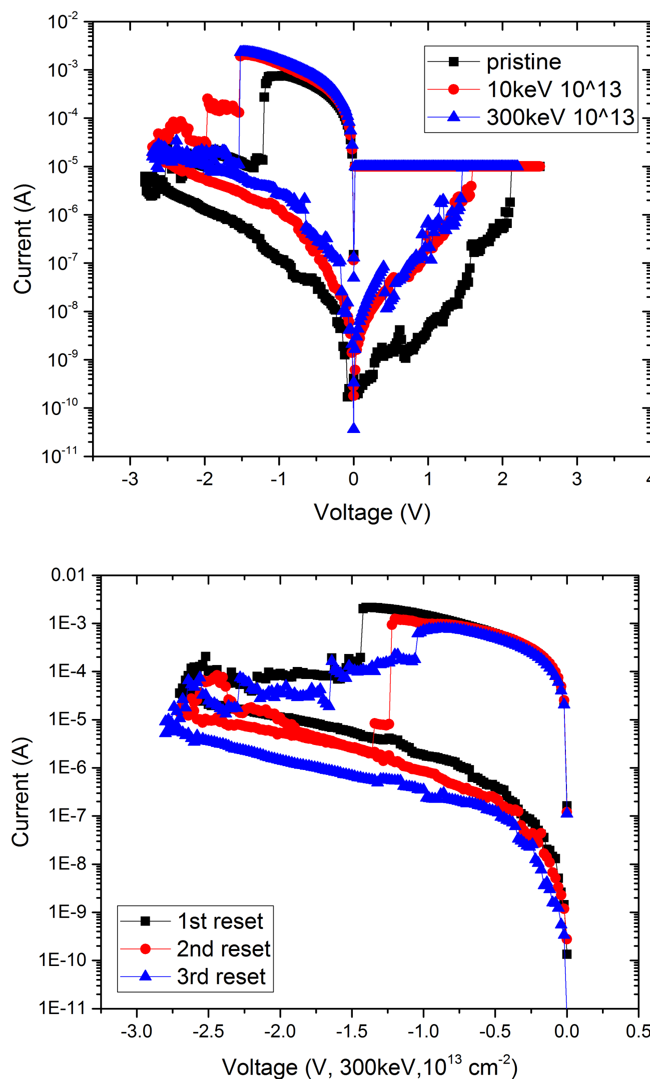

Figure 5. a) I-V characteristics of pristine and irradiated RRAM measured within a week after proton radiation; b) the first 3 reset cycles of a 300keV 10^{13} cm^{-2} proton-irradiated RRAM cell.

After a few months of storage at room temperature, the HRS resistance of 10, 100 and 300-keV proton-irradiated RRAM cells were measured as function of proton energy and fluence.

Figure 6 is the average HRS resistance measured at -0.5V of the RRAM cells irradiated with same fluence and different proton energies. About 20 samples are measured in each case, each RRAM cell was switched 5 to 10 times. They are plotted in both a linear (left) and a log scale (right). The graphs show that after proton radiation, the HRS resistance decreased compared with that of the pristine RRAM cells. Also, from the log-scale plot on the right, it can be seen that the HRS resistance is lower with higher proton energy. The 300-keV proton-irradiated samples show more significant differences before and after proton irradiation, while the 10-keV proton-irradiated case shows a smaller difference. This shows that the 300-keV protons generated more long-lasting damage that did than the 10-keV and 100-keVprotons. That is, the lower energy proton damage is recoverable.

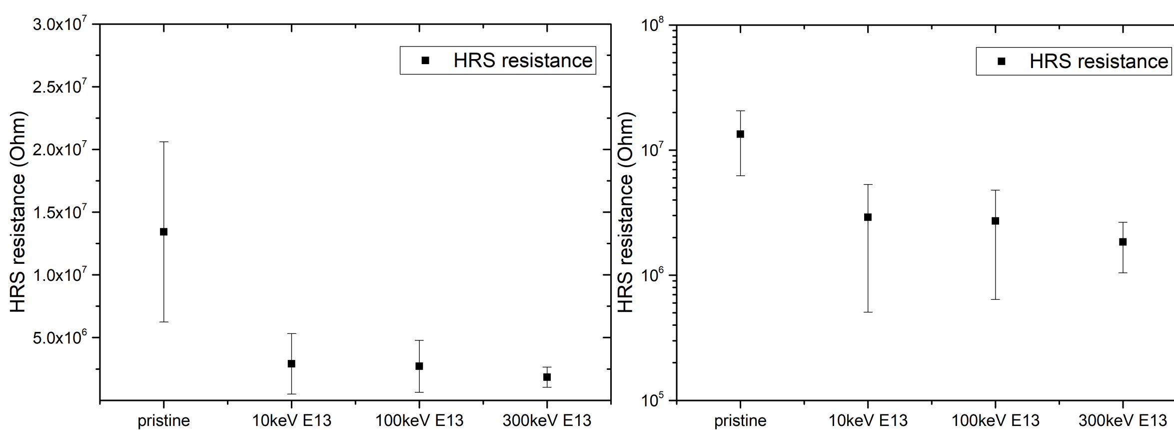

Figure 6. the HRS resistance as a function of proton energy.
Left: linear scale; right: log scale.

These results show that even though more oxygen vacancies are generated during lower-energy proton radiation, most of these radiation-induced-oxygen vacancies can recombine during the reset peocess. This is seen because those RRAM cells that are turned to LRS could be reset to HRS, which means that most of the radiation-induced-oxygen vacancies can recombine during the reset

process. Those radiation-induced defects that did not recombine during reset act as temporary electron trapping centers and affect the conductive filament's size.[7, 8, 9] Besides, in the HRS, there are more oxygen vacancies in the gap region of conductive filaments, as shown in Figure 7.[8] The extra oxygen vacancies can help to reconnect the filament under the set operation electric field.[10] This is the explanation of why the resistance of the HRS decreases after proton radiation.

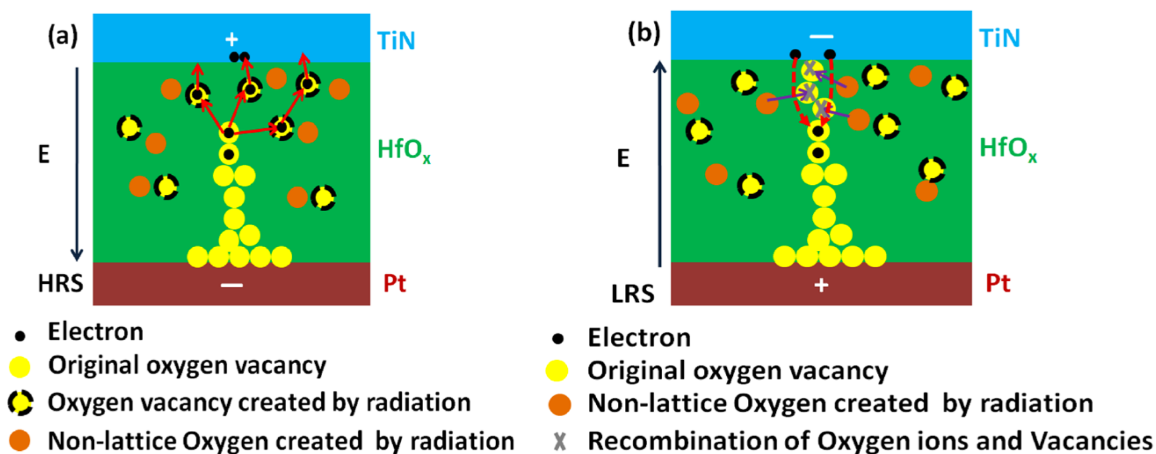

Figure 7. the effect of radiation on the RRAM's physical mechanism, (a) HRS and (b) LRS[8]

In order to examine the HRS resistance as a function of proton fluence, the middle proton energy 100keV was picked to expose the RRAM cells with higher fluences ranging from 10^9 to 10^{15} cm^{-2}. Figure 8 is the HRS resistance of RRAM cells irradiated with 100-keV proton radiation with different fluences. Left: linear scale; right: log scale. The fluences were chosen based on the maximum fluence obtained from the total ionizing dose (TID) level that the HfO_2-based memory can sustain.[10] Table 2 is the HRS resistance value of the sample exposed by each fluence. From the results, it can be seen that the HRS resistance decreases with higher fluence. This shows that more radiation-induced oxygen vacancies are generated by higher-fluence proton radiation.

Fluence	HRS resistance(kΩ)	variance	Standard deviation
Pristine	1.48×10^4	8.4×10^8	2.89×10^4
$10^9 cm^{-2}$	7.71×10^3	7.07×10^6	2.65×10^3
$10^{11} cm^{-2}$	5.34×10^3	8.65×10^6	2.94×10^3
$10^{13} cm^{-2}$	3.97×10^3	5.09×10^8	2.25×10^4
$10^{15} cm^{-2}$	3.24×10^3	9.74×10^7	9.86×10^3

Table 2. HRS resistance values of 100keV proton irradiated RRAM cells as a function of fluence.

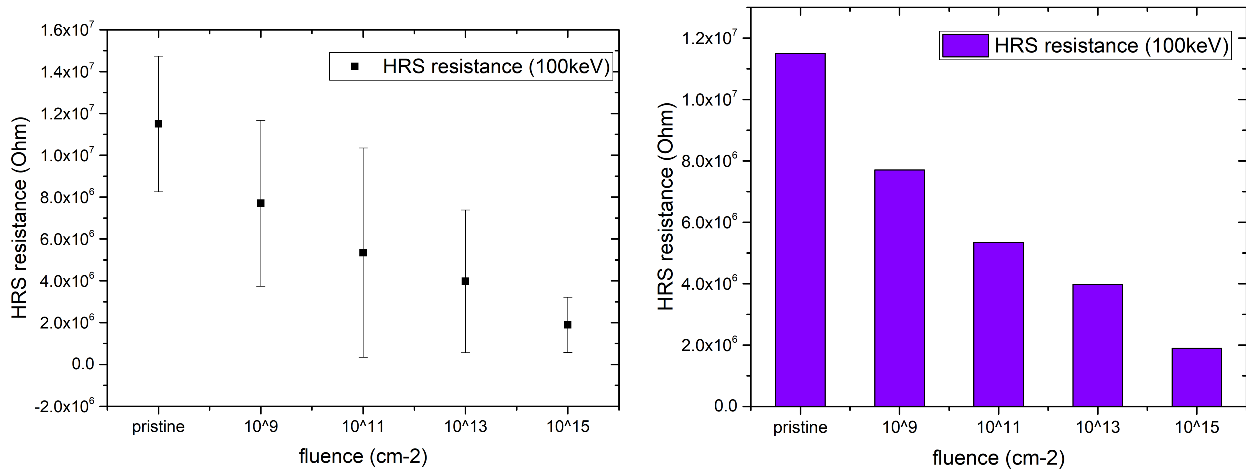

Figure 8. the HRS resistance as a function of proton fluence.
Left: linear scale, Right: log scale.

4. Damage Self-recovery at room temperature

As mentioned earlier, in order to determine if the proton radiation has long time effect on RRAM cells, the 10 and 300-keV proton-irradiated RRAM cells were measured twice. First:

within a week after proton irradiation, and second: 5 months after irradiation. Because the first measurement needed to be done as soon as possible and these measurements are time consuming, only the highest and lowest proton energy cases were used in this part.

After 5 months' of storage ("annealing") at room temperature, the HRS resistance of the 10 and 300-keV irradiated samples increased. Table 3 shows the comparison of the HRS resistance measured within a week and after 5 months. The 10-keV case shows the smallest change before and after room-temperature annealing, while the 300-keVcase shows the highest change. Figure 9 shows the comparison of the HRS resistance measured immediately after 300-keV, 10^{13} cm^{-2} fluence irradiation (first measurement) and 5 months after irradiation (second measurement). The HRS resistances were measured under 3 different bias. However, these values are still lower than those for pristine RRAM cells for all exposure conditions, which means the damage has only partially recovered at room temperature. The HRS resistance increased by 60% after 5 months.

	10keV $10^{13}cm^{-2}$	**10keV $10^{15}cm^{-2}$**	**300keV $10^{13}cm^{-2}$**	**300keV $10^{15}cm^{-2}$**
1 week	$1.71x10^{6}\Omega$	$6.95x10^{5}\Omega$	$6.1x10^{5}\Omega$	$6.7x10^{5}\Omega$
5 months	$2.34x10^{6}\Omega$	$1.48x10^{6}\Omega$	$1.84x10^{6}\Omega$	$1.08x10^{6}\Omega$

Table 3. HRS resistance of 10keV and 300keV proton irradiated RRAM measured within a week and after 5 months.

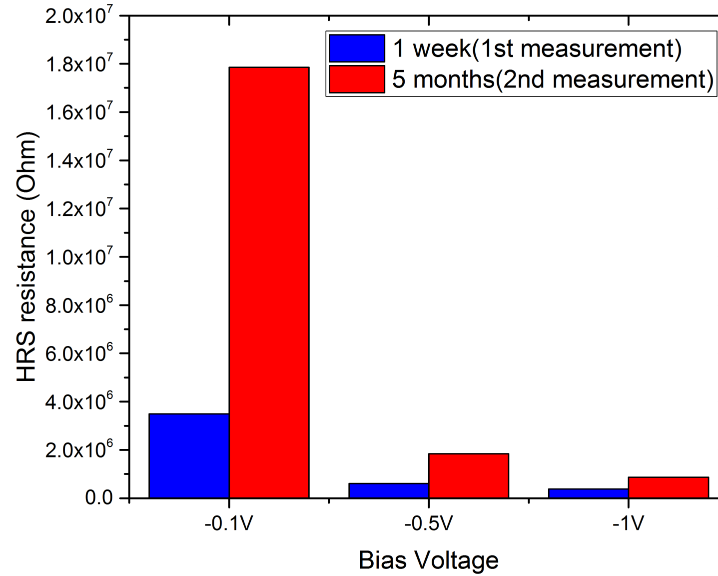

Figure. 9 Comparison of the HRS resistances as a function of bias. voltage. The pristine is compared in the next figure (Figure 10) where it shows that the resistance is still lower than pristine samples after recovery.

Figure 10 compares the average HRS resistance of pristine and 300-keV, 10^{13} cm^{-2} fluence proton-irradiated RRAM. The average HRS resistances calculated at -0.1V bias from the first and second measurements, are 3.49×10^{3} kΩ and 1.8×10^{4} kΩ respectively. The resistance value for the pristine sample is 5.1×10^{4} kΩ. as shown in Figure. 10. The average HRS resistances calculated at -0.5 V bias from the first and second measurements are 2.15×10^{2} kΩ and 9.38×10^{2} kΩ respectively. The value for the pristine sample is 1.48×10^{4} kΩ.

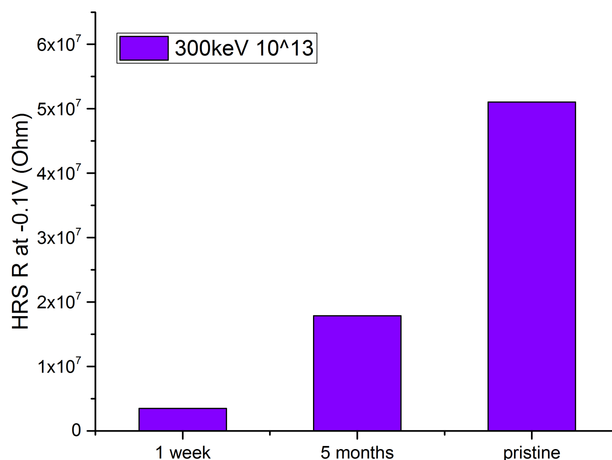

Figure.10 The average value of HRS resistances of pristine and 300-keV 10^{13} cm^{-2} fluence irradiated RRAM cells. The resistance increased after 5 months' storage ("annealing") at room temperature, but remained still smaller than the pristine sample.

The fact that some of the 10-keV proton-irradiated samples are formed and set to LRS is after irradiation likely caused by oxygen-displacement damage and O-Hf bond breaking[10 11]. The H ions incident on the film lose energy as they travel through HfO_2. The result of the energy loss is often the production of electron-hole pairs and displaced oxygen atoms (displacement damage). The displacement damage creates vacancies and interstitials. The electron-hole pairs are generated from ionization not displacement and the electron-hole pairs will recombine very fast.[9] The oxygen vacancies generated during proton irradiation at the interface may affect the forming process by changing the interface potential barrier.[30] In fact, forming-free RRAM (RRAM cells that don't need to be formed) using ion implantation with different kinds of ions has been reported in references[12, 13, 14]. Ti and Al ion implantation have been used in ZrO_2-based RRAM.[12] Oxygen-ion implantation has been used in Ta_2O_5 and HfO_2-based RRAM to obtain forming-free RRAM devices.[14] Ge doping has been used to obtain forming-free HfO_2-based RRAM.[14] The proton radiation in this work is same as H ion implantation. Forming free means those RRAM cells that

are formed after ion implantation do not need to be formed with a separate forming process. The displacement damage produces oxygen vacancies and interstitial oxygen atoms that contribute to the conductive filaments by acting as temporary trapping centers.[9,8,9] The high-energy proton radiation breaks up some of the Hf-O bonds, which can also result in oxygen vacancies and oxygen in interstitial sites.[5] During the reset process, some radiation-induced oxygen vacancy-interstitials can recombine under the influence of an electric field.[9] The change of resistance after radiation is likely from the segregation of radiation-induced defects.[6] However, defect reordering (annealing) can take place at room temperature**Error! Bookmark not defined.**, so the radiation-induced displacement damage decreases, and the crystal structure of the HfO_2 film can recover with time.[15] This might be the reason that after 5 months' annealing at room temperature, the HRS currents of irradiated RRAM cells have less variation between switching cycles.

B. Task five results from measurements on blanket films: The effect of proton radiation on HfO_2 blanket films

Next, in order to determine the cause of the damage on RRAM cells, and to prove the hypothesis, measurements will then be made on HfO_2 blanket films. This is a result of our hypothesizing that proton radiation will generate damage to RRAM. We further hypothesize this damage is generated from radiation-induced displacement. So in the tasks, we first examined if any RRAM has been damaged by proton radiation. Then we make measurements on blanket films to help determine the cause of the damage.

1. Electron-spin-resonance measurements

To determine possible damage mechanisms of the films, electron-spin-resonance measurements were made on 5-nm thick ALD HfO_2 blanket films on a Si substrate before irradiation (pristine) and after proton irradiation. As shown in Figure 11, only Si dangling bonds were detected in the pristine film. On the other hand, two defect states were detected from the proton-irradiated film: (1) Si dangling bonds as before and (2) oxygen vacancies. These results show that oxygen vacancies are generated during proton irradiation. In addition, the defect concentration of oxygen vacancies in the 10-keV proton-irradiated samples is higher than the 300-keV proton-irradiated samples. This can be seen from the results for oxygen vacancies in Figure 11 (b) and (c). These results are consistent with the TRIM-code simulation as shown in Chapter III. For low-energy exposure, more protons are likely to stay in the HfO_2 film and the 300-keV protons have enough energy to pass through the HfO_2 films and get to the substrate without doing as much damage as the lower energy protons. However, as mentioned earlier, the damage that is done by the 300-keV protons is more serious and often cannot be recovered.

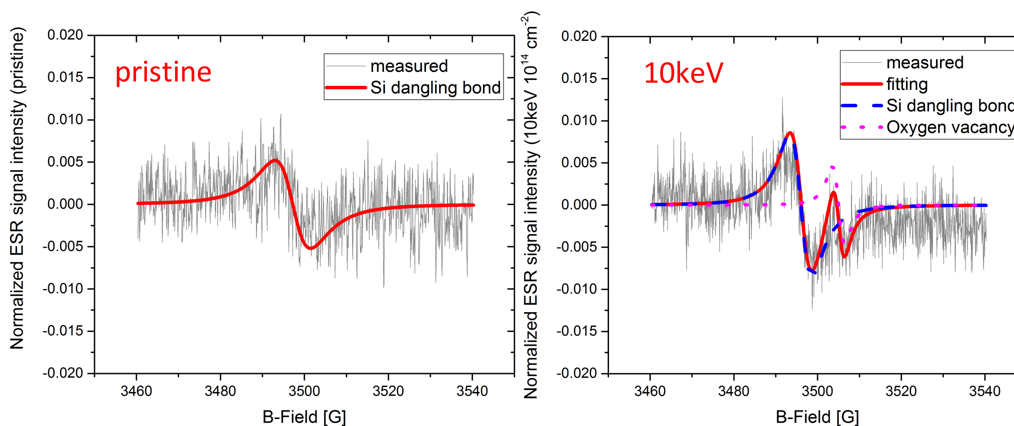

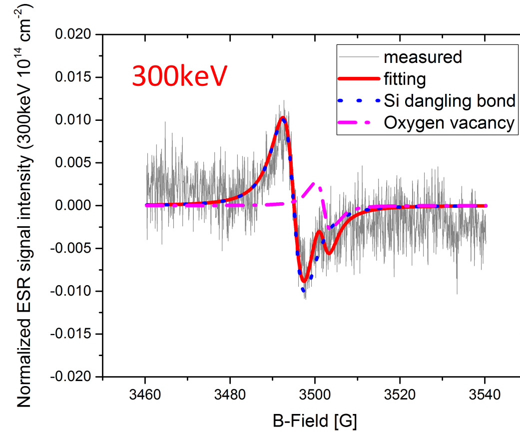

Figure 11. Measured Electron spin resonance and defect states fitting of (a). pristine, (b). 10-keV and (c). 300keV proton irradiated HfO_2 blanket films.

2. C-V and leakage current measurements

C-V characteristics can be used to determine the fixed oxide charge, interface defect states, dielectric constant and dielectric thickness. C-V measurements were made on both 5 and 100-nm thick HfO_2 blanket films with a MOS structure. For the proton-exposed samples, the HfO_2 film on Si substrate was exposed to proton radiation first and then a metal electrode was deposited on the HfO_2 film with vacuum evaporation. The metal electrode has a structure of 200-nm silver on top of 30nm titanium. The fixed oxide charge in the bulk and the interface charge will affect the shape of the C-V characteristics. The fixed oxide charge will affect the flat-band voltage of the C-V characteristics. The slope change of the depletion region of the C-V characteristics indicates the presence of interface defect states.[16] Figure 12. shows the C-V characteristics of the pristine and 10-keV proton-irradiated HfO_2 films with different thicknesses: 5 nm (left) and 100 nm (right).

First, the value of C_{ox} under negative bias shows a 50% decrease in value in the 5-nm HfO_2 film after 10-keV and a fluence of $10^{14}cm^{-2}$ proton exposure. All CV characteristics are measured at room temperature. The oxide capacitance C_{ox} is related to the dielectric thickness d and the dielectric constant k by the expression $C_{ox} \approx \frac{Ak\varepsilon_0}{d}$, where A is the area and ε_0 is the vacuum permittivity. This change can come from the decrease of the k value or an increase of the thickness of the oxide layer or both. However, the C-V characteristics of 100-nm HfO_2 sample shows that the value of C_{ox} is about the same before and after proton irradiation.

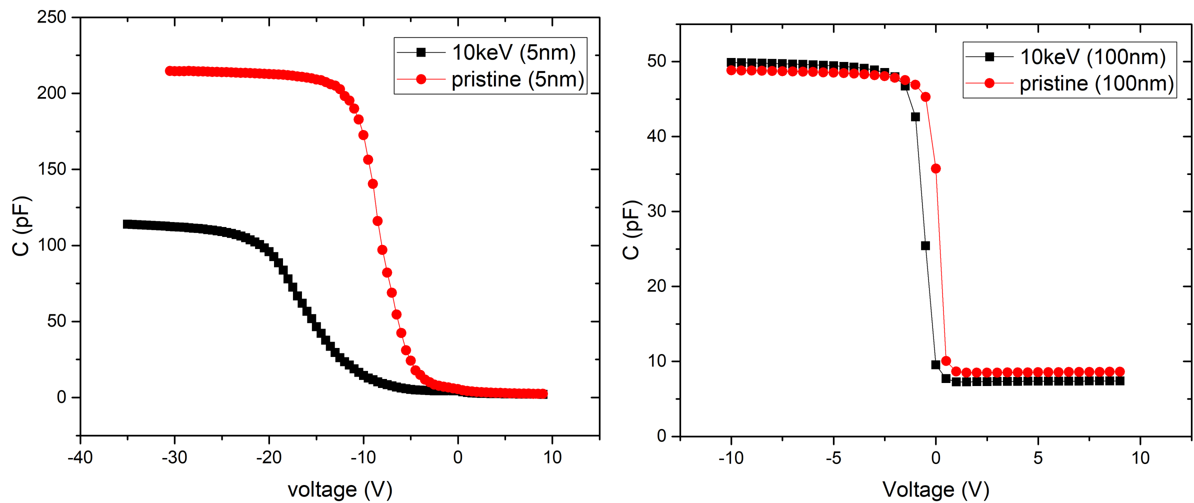

Figure 12. High frequency C-V characteristics of 5nm(left) and 100nm(right) HfO_2 films.

The same setup for the CV measurements can also be used to measure leakage currents. As is well known, the capacitance and conductance of an object are duals of each other. That is, by replacing the permittivity with conductivity, the same expression can be used to calculate the conductance of the object. The leakage-current measurements on the MOS structure can thus be easily made.

To confirm this, as shown in Figure 13, the leakage currents for 5-nm and 100-nmHfO_2 blanket films show similar results as the CV measurements. The leakage current of the 5-nm blanket film decreases after 10-keV proton irradiation, indicating that the conductivity increases. However, the leakage current of the 100-nm blanket film did not change before and after proton radiation. This indicates that both the changes in capacitance and conductance occur at the interface of the films with the electrodes.

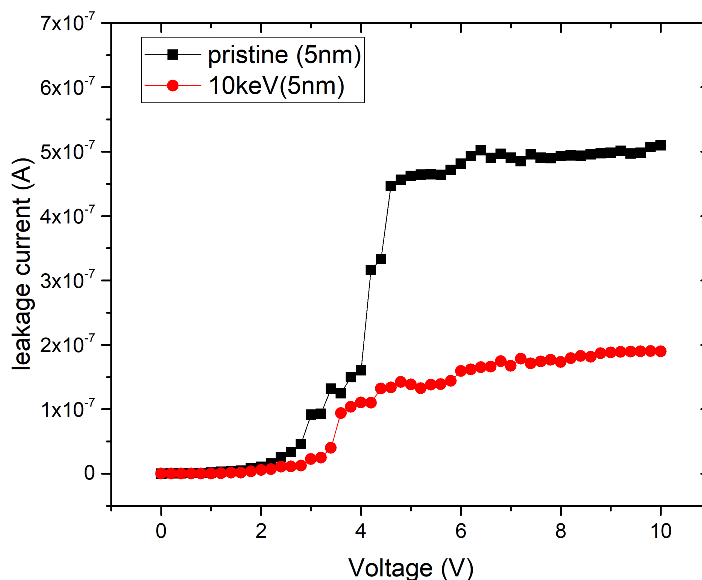

Figure 13. leakage current measurements of 5-nm HfO_2 film.

The film crystallization structure of the HfO_2 film is closely dependent on the film thickness.[17, 18, 19] The XRD results shows that the film structure isn't changed after proton radiation from 10keV to 300keV. This shows that the thickness of the 100-nm HfO_2 film isn't significantly changed after proton radiation. Therefore, there is no significant change on the k value or the thickness of the 100-nm HfO_2 film after proton irradiation. Thus, the decreasing of C_{ox} of the 5-nm HfO_2 sample after proton irradiation is most likely from the fact that a thin layer of oxide is generated in the HfO_2/Si interface after proton irradiation (as shown in Figure 14). Oxygen vacancies and oxygen

atoms (and/or oxygen ions) are generated during proton irradiation. Oxygen is then released from both the 5-nm and 100-nm films and moves into the Si substrate.[20] Since the 5-nm HfO_2 film is very thin, most of the defects are generated in the interface. It is likely that the same effect occurs with the 100-nm thick film, but the result only changes the capacitance by a virtually undetectable amount since the capacitance of the bulk is so much smaller than that of the interface. Note the equivalent circuit of the film with the oxide layer is that of two capacitors in series. The 5-nm film capacitance is much larger than the 100-nm capacitance, so the thin layer oxide capacitance has a much larger effect. The identical argument can be made for the conductance measurements.

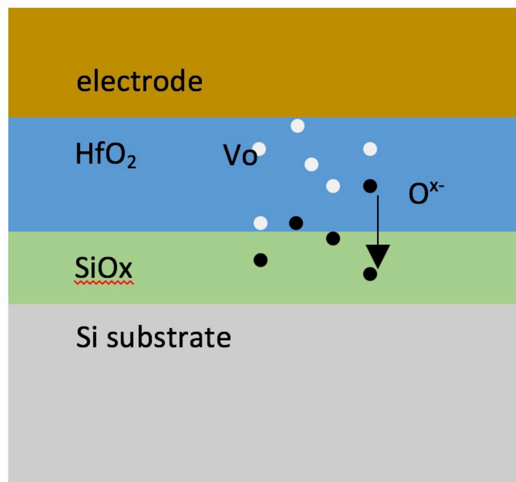

Figure 14. Shows how oxygen atoms are released from the hafnium oxide and move into the substrate and thus the silicon surface is being oxidized.

The flat-band voltage shift is often used to determine whether there are fixed defect states present in the bulk of dielectric film. In order to show the flat-band voltage shift and the charge accumulation, a normalized C/C_{ox} ratio C-V curves of both the pristine and 10-keV proton irradiated HfO_2 film are plotted in Figure 15. It shows that there is a lateral leftward shift in the C-

V curve of the 10-keV proton irradiated sample. The left shift means that there are fixed defect states which are positively charged are generated in the oxide after proton irradiation.[21]

In addition to the flat-band voltage shift, there is also a slope change in the C-V curve after proton-irradiation. The “changed” C-V curve of the proton-irradiated sample shows that interface traps are present after proton irradiation.[22] These interface traps behave very much like bulk deep-level traps and can have energy levels in the bandgap of the oxide.[22]

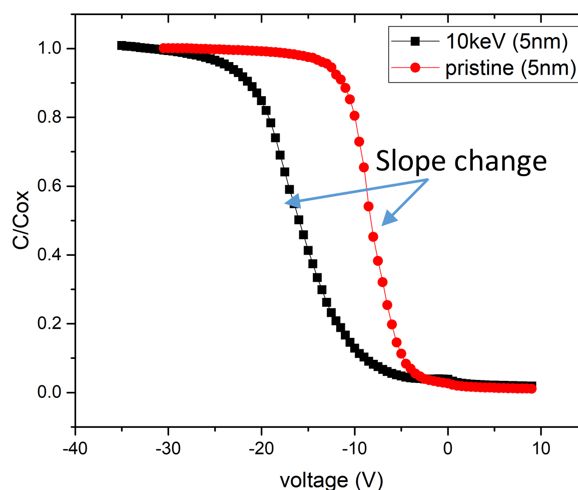

Figure 15. normalized C-V curve of pristine and 10-keV proton-irradiated 5-nm HfO_2 samples. In Figure 13, no such changes were seen in 100nm HfO_2 samples.

3. X-Ray diffraction XRD

To determine whether the crystal structure of HfO_2 is changed after irradiation, samples with 100-nm thick ALD HfO_2 blanket films on Si substrate were measured with XRD. The HfO_2 film is monoclinic polycrystal and the measurements were made with a Bruker D8 Discover diffractometer. Figure 16 shows the XRD results for pristine and proton-irradiated polycrystalline HfO_2 films. The HfO_2 blanket films have the structure as the HfO_2 in RRAM. The XRD results

show that the crystal orientation was *not* changed by the proton radiation with energies of 10-keV or 300-keV. The XRD measurements were made at two different times: 1). within a week and 2). 5 months after after proton irradiation. The results of these two measurement are same.

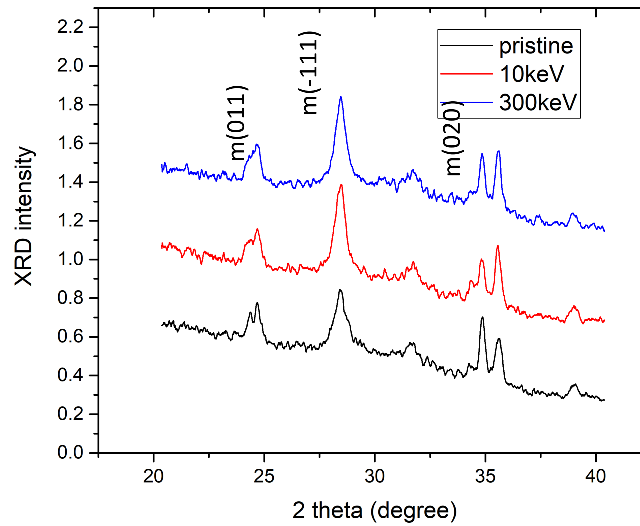

Figure 16. XRD measurement results of pristine and proton irradiated polycrystalline HfO_2 film.

C. Tasks two, three, and four: Results from endurance and retention measurements:

1. Endurance

a. Endurance measurements of pristine samples and endurance failure.

Figure 17 shows the endurance of the pristine RRAM cells. The pristine HfO_2 RRAM cells have endurance up to 3M cycles measured under the conditions explained in Chapter IV. The

endurance of the same HfO_2-based RRAM (non-irradiated) has been reported in reference [23] . The results showed in reference 23 indicate that this pristine HfO_2-based RRAM has good endurance (up to 10^9 cycles).

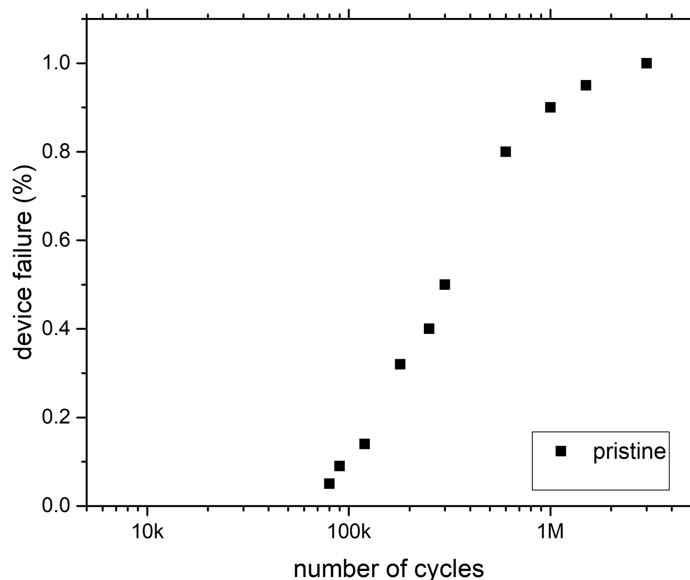

Figure 17. Endurance of pristine RRAM devices.

Figure 18 a) shows the measured I-V Characteristics and Figure 18 b) shows the HRS and LRS resistances during repeated switching cycles of a pristine RRAM cell. From Figure 18 a), it can be seen the HRS current increased slightly as the number of switching cycles increased, which means the HRS resistance decreased as the number of switching cycles increased. However, within ~10^6 cycles, no significant degradation of the ON/OFF window or set/reset voltage is seen for those devices still operating.

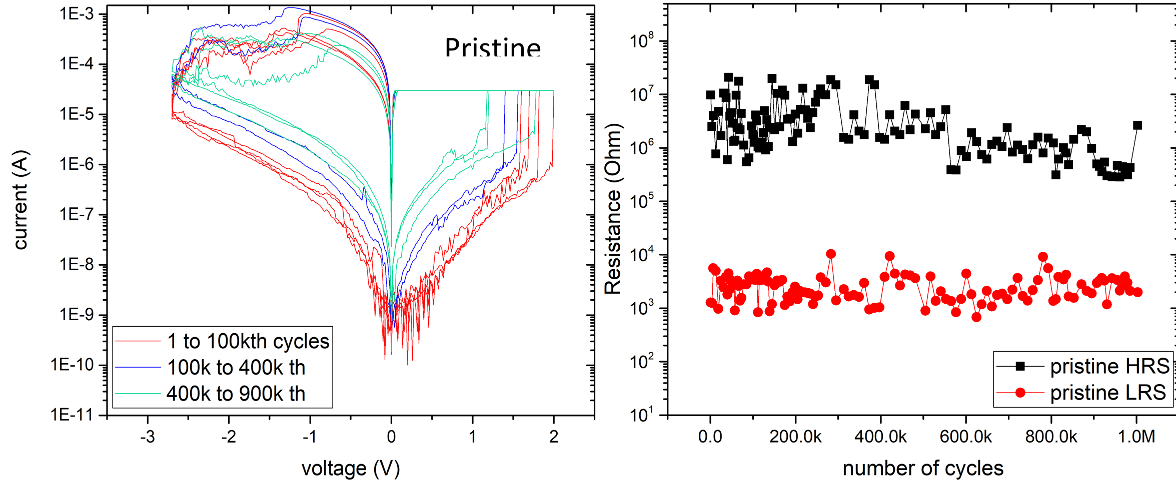

Figure 18. a). measured I-V characteristics and b). HRS and LRS resistance of pristine RRAM cell as a function of switching cycles.

Generally, the number of endurance cycles of RRAM depends on a variety of factors, *e.g*, materials, structure, write voltage and frequency[24, 25]. Therefore, these conditions were set to be constant, as listed in chapter IV, for the measurements of different radiation cases. Thus, we know the observed differences between samples are from the proton radiation. Usually , the final failure state of RRAM is that it is stuck in the LRS state and unable to reset back to HRS.[26] The reason for this could be that too many defects such as oxygen vacancies have accumulated during the cycling. There are two locations where this can happen 1). at the electrode/oxide interface; 2). near the filament in the oxide layer.[27] These can happen at the same time.

There are also two types of RRAM endurance failures that were measured in this work The first type of endurance failure is due to a small ON/OFF ratio (decreased R_{HRS} and increased R_{LRS}) as shown in Figure 19. The other type of endurance failure is due to dielectric breakdown so that the RRAM can no longer be reset during switching. Only the second type endurance failure was measured with pristine RRAM cells. Both types of endurance failure were measured with the

proton-irradiated RRAM cells.

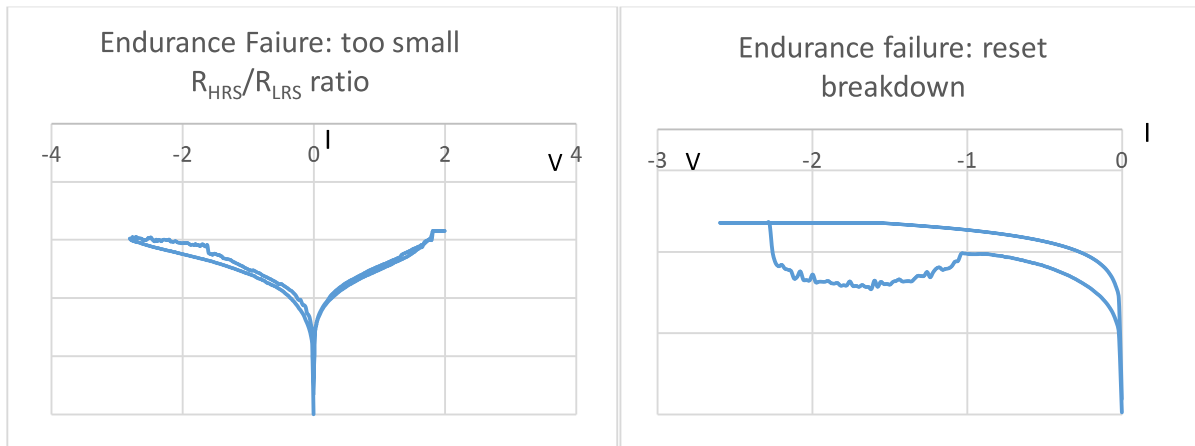

Figure 19. a). endurance failure due to small R_{HRS}/R_{LRS} ratio;
b). endurance failure from dielectric breakdown.

In the SET process, the conductive filaments are formed from the generation of oxygen vacancies and oxygen ions. Then the oxygen ions drift to the anode (top electrode) and are stored in the electrode under positive bias.[27] In a typical RESET process, the stored oxygen ions in the electrode layers can be moved to the resistive switching layer from the top electrode to rupture the conducting filament when the device is under reverse bias. This nature of this reset process has been previously explained in Chapter II.

The oxygen ions produced during the SET/RESET switching process can cause oxidation at the anode and electrode interfaces.[24, 27] This interface oxidation will increase the LRS resistance, as explained in chapter II. In addition, extra oxygen vacancies generated in the HfO_2 film during proton radiation and set process under the forward electric fields increase the filament size and decrease the HRS resistance.[31]

b. Endurance as a function of proton energy

Figure 20. shows the endurance of the pristine and the proton-exposed RRAM cells. The proton-exposed RRAM cells are irradiated with different proton energies and the same fluence (10^{14} cm^{-2}). Under the same measurement conditions, the pristine HfO_2 RRAM cells have endurances up to $3*10^6$ cycles. After proton irradiation the endurance decreases, especially the 50% endurance failure point. In addition, the 50% endurance failure decreases with higher proton energy. For the pristine RRAM samples, 50% of the cells failed below 300k cycles. 50% of the 300keV proton irradiated RRAM cells failed below 100k cycles, around 50% of the 100keV and 10keV proton irradiated RRAM cells failed below 180k cycles. To extrapolate to real time, the endurance is measured at different temperatures and the results are then extended to room temperature. The high-temperature measurements are presented in next section.

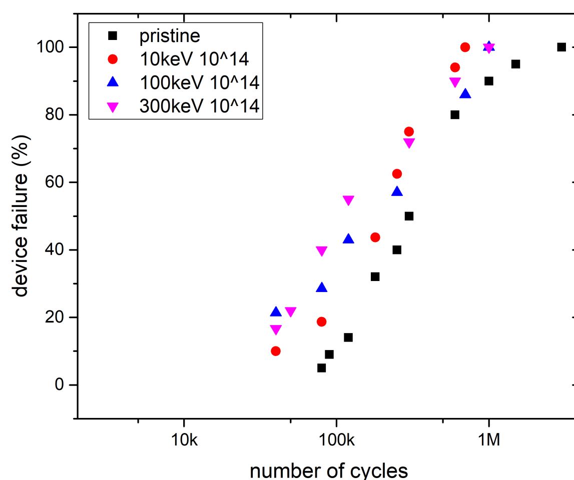

Figure 20. Endurance of pristine and proton exposed RRAM devices. The proton energies are 10keV ,100keV and 300keV.

Figure 21 shows a comparison of the a) pristine and b) 300-keV proton-irradiated RRAM cells' resistance endurance characteristics up to 10^6 cycles. Good uniformity of switching

parameters such as LRS and HRS resistance was measured in pristine RRAM cells. Within 10^6 switching cycles, there is no significant decrease of the ON/OFF ratio (It is also called the logic window) in pristine RRAM cells. The ON/OFF ratio of pristine RRAM is about 10 times smaller after 10^6 switching cycles. However, for the 300-keV proton-irradiated RRAM cells, the HRS resistance *decreased* by two orders of magnitude after 10^6 switching cycles. The LRS resistance of 300-keV proton irradiated RRAM cells *increased* about 5 times after 10^6 switching cycles. Finally, the ON/OFF ratio is about three orders of magnitude smaller after 10^6 switching cycles (as shown in Figure 21 b). This means after proton radiation the ON/OFF ratio are decreases faster with more switching cycles.

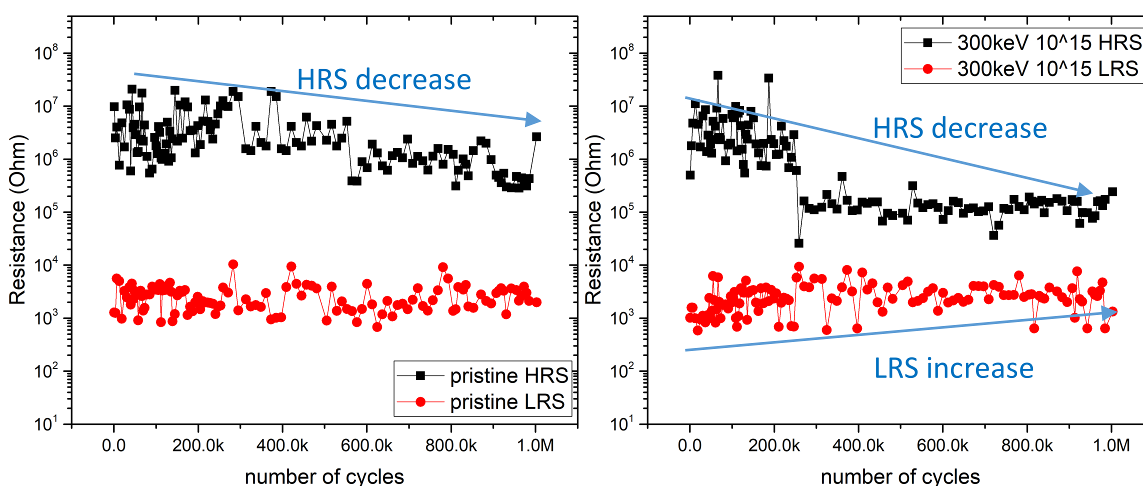

Figure 21. measured HRS and LRS resistance of a) pristine and b) 300keV proton irradiated RRAM as a function of switching cycles. The LRS resistance of proton exposed RRAM cells is 5 times smaller and HRS resistance is 100 times smaller after 1 M cycles.

Figure 22 is the measured I-V characteristic of a 300-keV proton-irradiated RRAM cell up to 10^6 switching cycles. As compared with the I-V characteristics of a pristine RRAM cell in Figure 18 a), the proton-irradiated RRAM cell shows greater HRS resistance decrease with as the number of switching cycles increased. It is likely that the HRS changes comes from the

number of the ruptured CFs (conductive filaments) length (physical gap of the CFs as shown in Figure 23) [28] . In the LRS state, there is no gap, so that the change is less significant for the LRS resistance than the HRS.[28, 29]

The radiation-induced charge-trapping centers add energy levels in the HfO_2 bandgap.[Error! Bookmark not defined., 30] In addition, the radiation-induced defects in the devices may affect the CFs' size, length and the filament growth activation energy E_a.[31] The increased CFs size may also cause RESET failure.[32] The uncombined proton-induced oxygen vacancies and defects serve as electron trapping centers in the HfO_2 film and make the dielectric material easier to break down.[30] Furthermore, the H ions can reduce the filament-formation energy. The higher the concentration of H ions, the greater the reduction of the filament-formation energy.[33] Therefore, the endurance cycles of proton-irradiated RRAM decrease with higher proton energy.

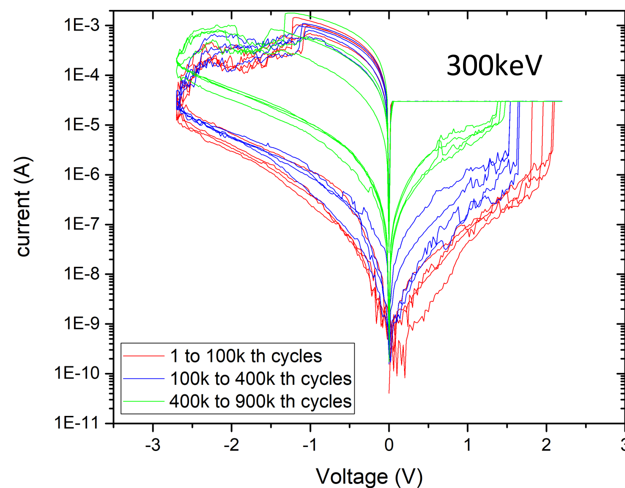

Figure 22. measured I-V characteristics of one 300-keV proton irradiated RRAM cell up to 10^6 switching cycles.

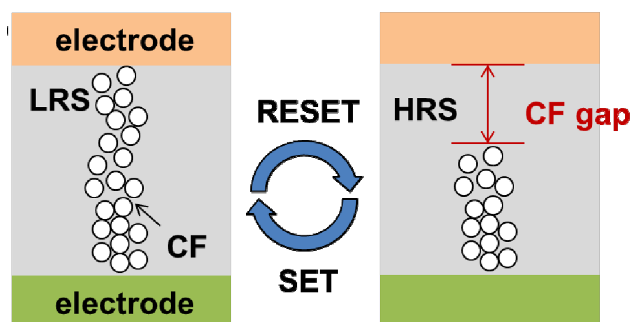

Figure 23. Conductive filaments in HRS and LRS.[28]

c. Endurance as a function of proton fluence

The endurance was also measured as a function of fluence. Table 4. shows that the endurance failure percentage of RRAM cells that are exposed with 100keV proton energy over a range of proton fluences. The fluences are: 10^{9}, 10^{11}, 10^{13}, 10^{14} and 10^{15} cm^{-2}. Table 3 and Figure 24 shows that when the fluence is less than 10^{13} cm^{-2}, the endurance is not significantly affected by the proton irradiation. However, when the fluence is higher than 10^{13} cm^{-2}, the endurance slightly decreases compared with the pristine RRAM cells.

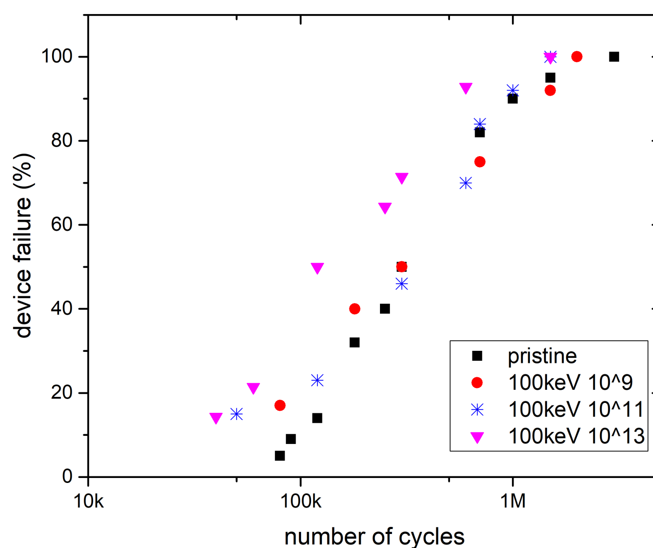

Figure 24. Measured endurance of 100-keV proton-exposed RRAM cells as a function of proton fluence.

Number of cycles	pristine	100keV $10^9 cm^{-2}$	100keV $10^{11} cm^{-2}$	100keV $10^{13} cm^{-2}$	100keV $10^{14} cm^{-2}$	100keV $10^{15} cm^{-2}$
<60000				0.2	0.25	0.25
<90000		0.2				
<120000	0.15		0.25	0.5	0.4	0.4
<180000	0.3	0.4				0.5
<250000	0.4			0.6	0.6	0.75
<300000	0.5	0.5	0.5	0.7		
<600000	0.8		0.7	0.9		0.9
<800000		0.8			0.9	
<1000000	0.9	0.9	0.9		1	1
<1500000			1	1		
<2000000		1				
<3000000	1					

Table 4. Endurance failure rate of 100-keV proton exposed RRAM cells as a function of fluence.

Figure 25. show that when the fluence is higher than $10^{13}cm^{-2}$, the endurance of the 10-keV, 100-keV and 300-keV proton-irradiated RRAM cells all decrease compared with pristine RRAM cells. The endurances of proton-exposed samples with different fluences is very close and 50% failure happens in about same range. The endurance values for each proton energy are given in the previous section. This is designed to show the endurance decreases after proton

irradiation compared with the pristine RRAM cells.

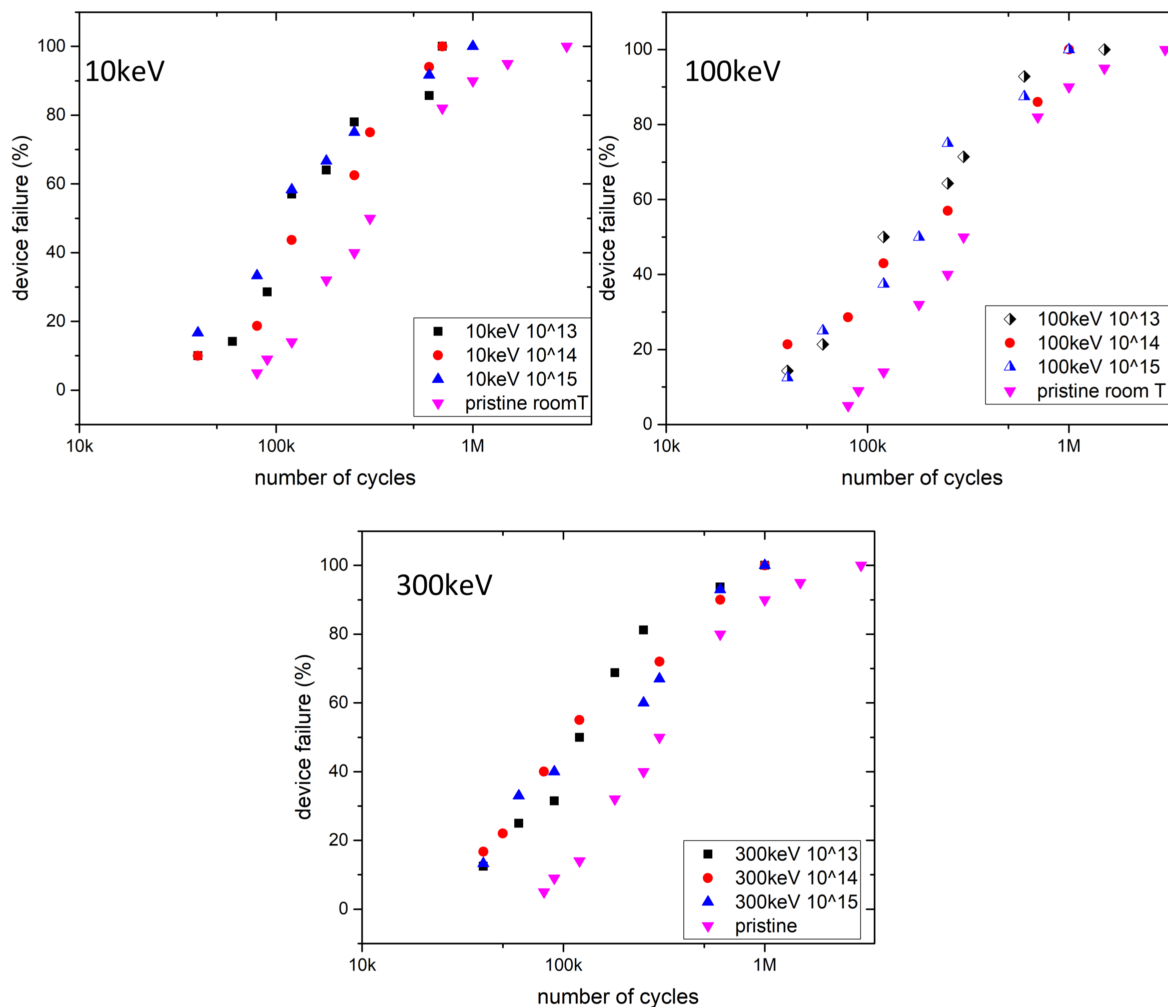

Figure 25. Measured endurance of 10 to 300-keVproton-irradiated RRAM cells as a function of fluence.

d. Endurance as a function of temperature

The endurance of pristine and proton-irradiated RRAM cells was measured at four temperatures: room temperature, 75, 120 and 150 °C. A hot plate was used for the high temperature measurements as shown in Figure 26. The temperature of the samples could be manually controlled.

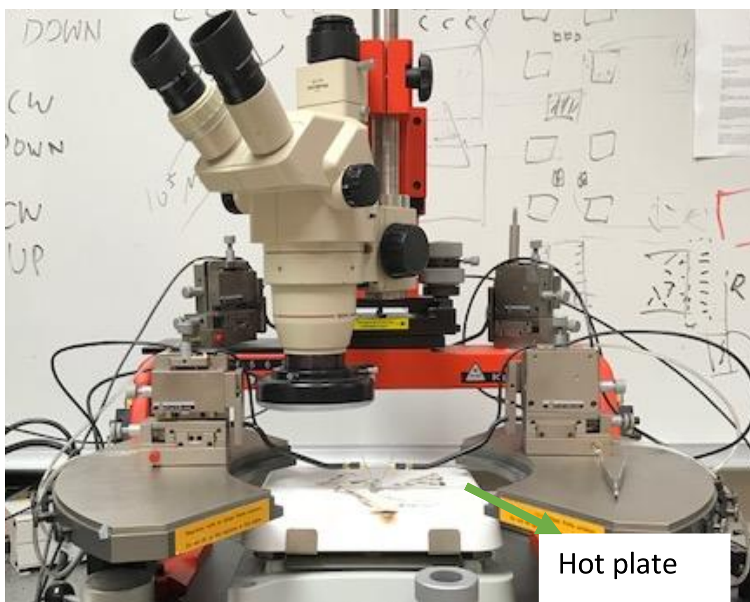

Figure 26. The hot plate and probes used for high-temperature measurements.

Figure 27 shows the endurance characteristics of pristine RRAM measured at different temperatures. The endurance of pristine RRAM cells decreases as the temperature increased. It is clear that more pristine RRAM devices fail earlier at higher temperatures.

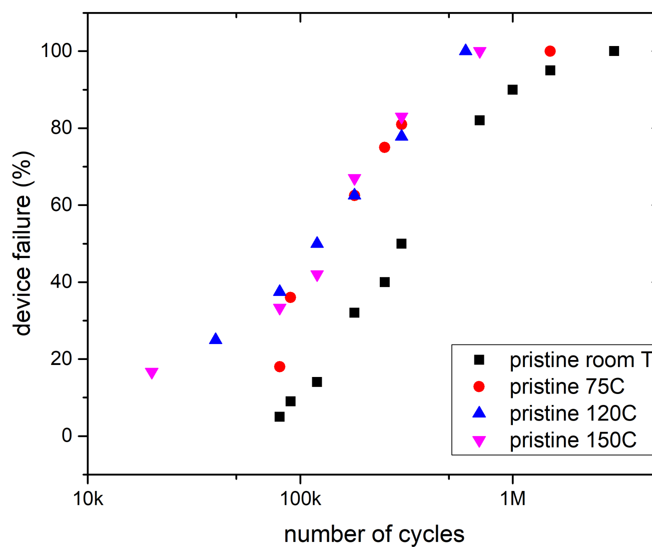

Figure 27. Endurance characteristics of pristine RRAM as a function of temperature.

A comparison of resistive switching measured at room temperature and 150°C is shown in Figure 28. It is observed that the HRS current increases at high temperature. The LRS current under positive voltage is the compliance current so that it is always held constant. Since the HRS current at 150°C is higher than at room temperature, the compliance current needed be set to a higher value in order to make sure the device can be successfully set. The compliance current can be set in the semiconductor parameter analyzer. When the device is reset to HRS, the conductive filaments are broken near the dielectric/electrode interface (as shown in Figure 6), and the gap between the conductive filaments and the electrode limits the current (HRS current).[34]

The oxygen-vacancy generation probability (when the applied voltages are constant) can be expressed as[35, 34]:

$$p \propto \exp\left(-\frac{E_a}{k_B \mathrm{T}}\right) \qquad (1)$$

where E_a is the activation energy for the formation of oxygen vacancies, k_B is Boltzmann's constant and T is the temperature in degrees Kelvin. With increasing temperature, the probability of oxygen-vacancy formation increases. The increased oxygen-vacancy-related trap density at high temperature can enhance the trap-assisted tunneling current at HRS.[34, 36, 37] Thus, the HRS current increases at high temperature. In addition, the oxygen-ion mobility will increase with increasing temperature.[34] Since the probabilities of creating oxygen vacancies and the oxygen ion mobility are both increased at higher temperature, the set and reset voltage will decrease with increasing temperature.

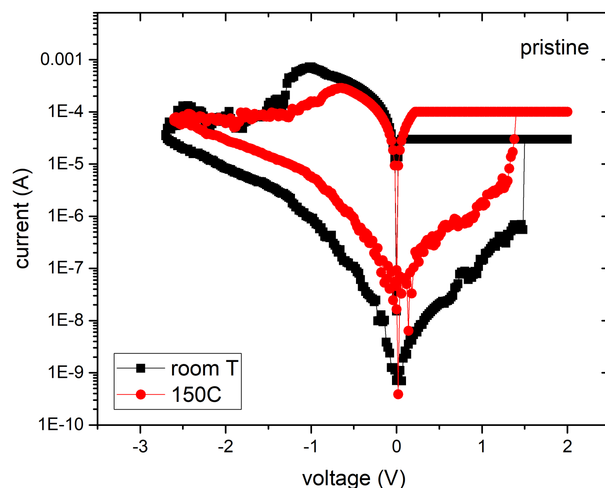

Figure 28. Comparison of resistive switching at room temperature and 150°C.

The high-temperature endurance characteristics of the proton-exposed RRAM are shown in Figure 29. In Figure 29 (a) and (b), the 10-keV and 100-keV proton-irradiated RRAM cells' endurance cycles (until failure) decrease at higher temperatures. The degradation of endurance at high temperature is less significant in the RRAM cells that are exposed with 100-keV than 10-keV. However, in Figure 29 (c), the endurance of 300-keV proton-exposed RRAM cells measured at high temperature and room temperature are very close, except that more 300-keV proton irradiated RRAM cells fail before 50k switching cycles at 150°C.

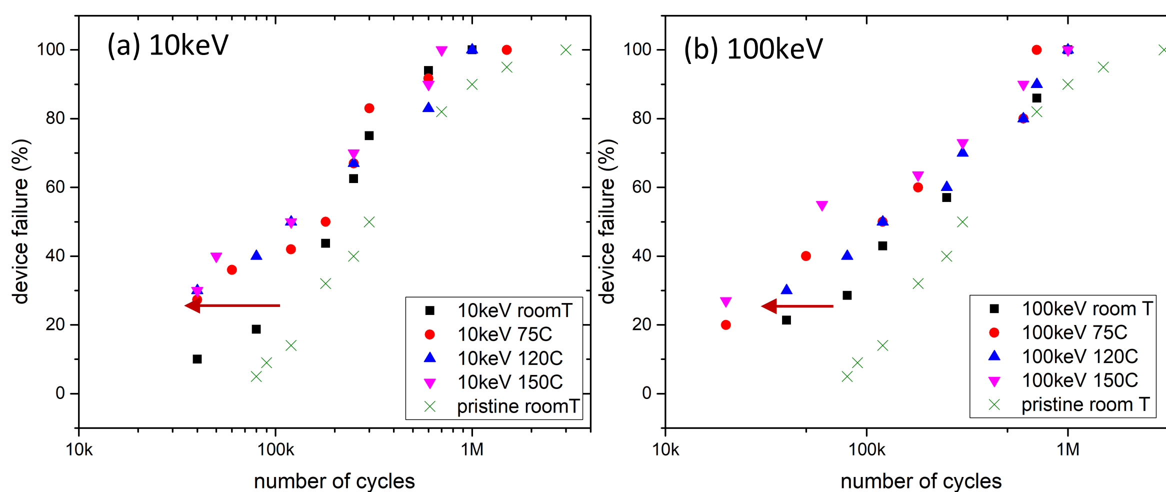

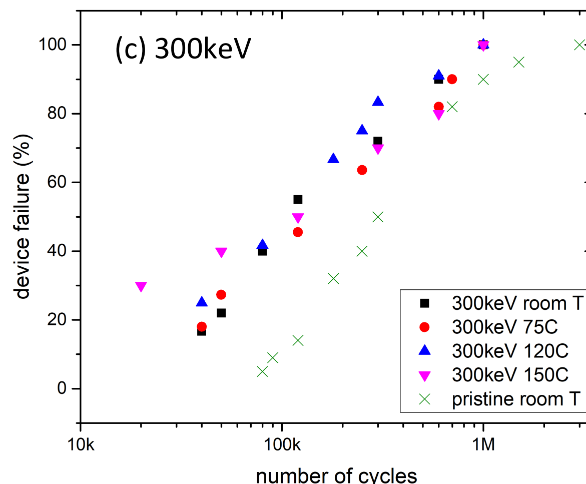

Figure 29. Endurance of proton-irradiated RRAM cells a) 10-keV, b) 100-keV and c) 300-keV measured at high temperatures.

Figure 30 (a) shows the 600k cycle endurance test of a 100-keV proton irradiated RRAM cell measured at room temperature and (b) at 150°C. The HRS and LRS resistance are read at -0.5V. It was observed that the resistance uniformity of each measurement is better at room temperature than at 150°C. The variance between Max and Min value of HRS resistance measured in room temperature is about 100, and at 150 °C, the variance is about 2000. This is because oxygen-ion diffusion is enhanced at high temperature. The diffused oxygen-ions recombine with oxygen vacancies randomly in the dielectric film. Therefore, the size and length of the conductive filaments are affected by oxygen-ion diffusion.

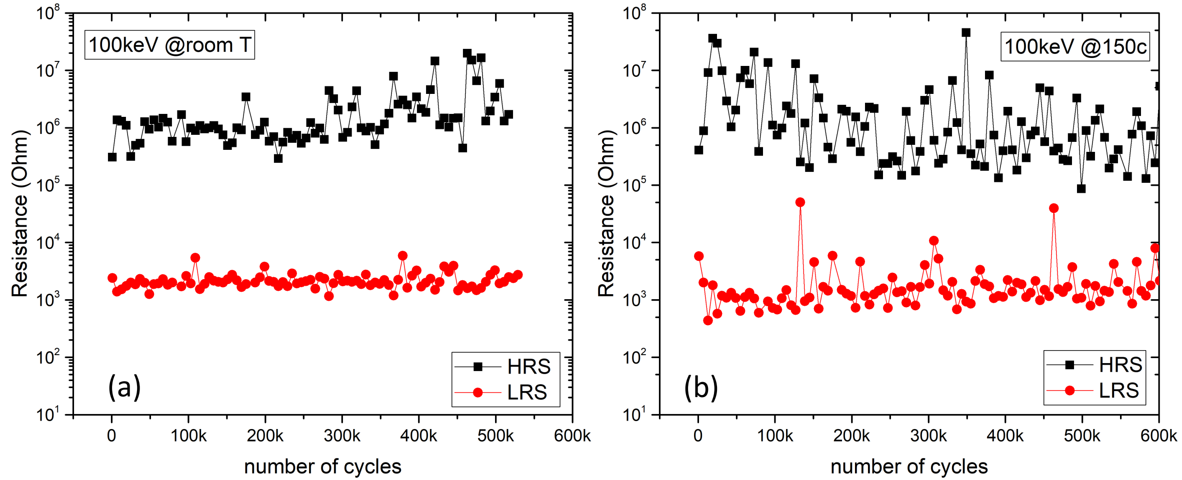

Figure 30. HRS and LRS resistance of a 100-keV $10^{14}cm^{-2}$ proton-irradiated RRAM cell measured at a) room temperature and b) 150°C with repeated switching cycles. The variance of HRS resistance measured in room temperature is about 100 times, and at 150 °C, the variance is about 2000 times.

As shown earlier, the HRS resistance decreases with higher proton energy. This means that during resistive switching, there are more unrecoverable radiation-induced defects in 300-keV proton-irradiated RRAM cells than for the lower proton energies. These defects enhance the electron hopping and lower the formation energy E_a.[38, 39] Based on crystal defect and probability theories, the cumulative-failure probability (time-dependent failure probability) can be expressed as a function of applied voltage and defect-generation probability.[35, 40, 41, 42] The oxygen-vacancy generation probability is shown in Eq (1). A low E_a value exhibits a weak temperature-dependence of the dielectric breakdown.[43] Since the E_a value is smaller after higher proton irradiation,[33] the 300-keV proton-irradiated RRAM cells have the smallest E_a value. Thus, the endurance of 300-keV exposed RRAM cells shows less difference between the measurements at different temperatures.

2. Retention

The LRS retention was measured for the pristine, 10, 100 and 300-keV proton-exposed RRAM cells at 120°C. The samples exposed with the highest fluence (10^{15} cm^{-2}) were used for the retention measurements. In order to accelerate the retention test, a high temperature of 120°C and a read voltage of 0.5V were used in the retention measurements. As shown in Figure 31, all the measured RRAM cells can still be set and reset after >10^5 s (more than 8 hours) retention measurement. Based on the accelerated reliability testing model described in references [44] and [45], higher temperature and higher voltage would speed up the failure. The 8-hour retention time measured in this situation can be extrapolated to about 14-15 years' lifetime. These results show that after proton exposure, the RRAM cells still have very good retention behavior.

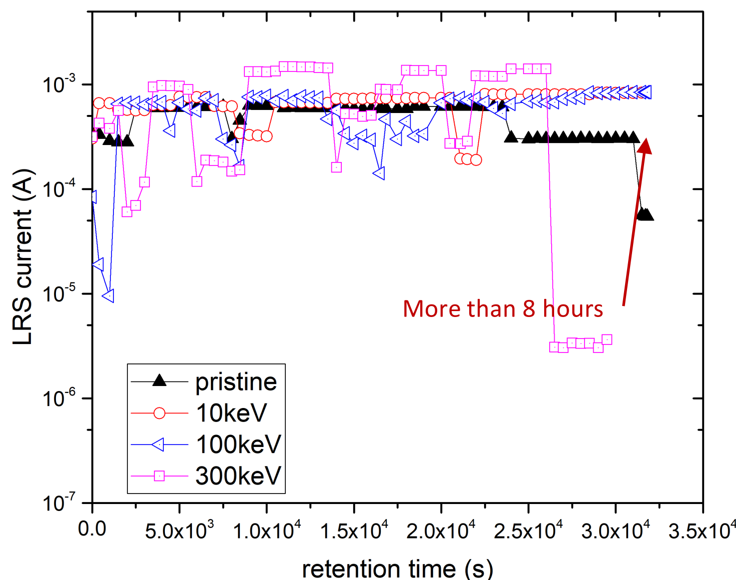

Figure 31. Retention time of pristine and proton irradiated RRAM cells at 120°C.

References

[1] Zhang, Haowei, Bin Gao, Bing Sun, Guopeng Chen, Lang Zeng, Lifeng Liu, Xiaoyan Liu et al. "Ionic doping effect in ZrO 2 resistive switching memory." *Applied Physics Letters* 96, no. 12 (2010): 123502.

[2] Felix, J. A., J. R. Schwank, Daniel M. Fleetwood, M. R. Shaneyfelt, and Evgeni P. Gusev. "Effects of radiation and charge trapping on the reliability of high-k gate dielectrics." *Microelectronics Reliability* 44, no. 4 (2004): 563-575.

[3] Fang, Runchen, Yago Gonzalez Velo, Wenhao Chen, Keith E. Holbert, Michael N. Kozicki, Hugh Barnaby, and Shimeng Yu. "Total ionizing dose effect of γ-ray radiation on the switching characteristics and filament stability of HfOx resistive random access memory." *Applied Physics Letters* 104, no. 18 (2014): 183507.

[4] Bi, J. S., Z. S. Han, E. X. Zhang, M. W. McCurdy, R. A. Reed, R. D. Schrimpf, D. M. Fleetwood et al. "The Impact of X-Ray and Proton Irradiation on HfO2/Hf-Based Bipolar Resistive Memories." *IEEE Transactions on Nuclear Science* 60, no. 6 (2013): 4540-4546.

[5] Fang, Z., H. Y. Yu, X. Li, N. Singh, G. Q. Lo, and D. L. Kwong. "HfO2/TiOx/HfO2/TiOx Multilayer-Based Forming-Free RRAM Devices With Excellent Uniformity." *IEEE Electron Device Letters* 32, no. 4 (2011): 566-568.

---

[6] Kim, Wonjoo, Alexander Hardtdegen, Christian Rodenbücher, Stephan Menzel, Dirk J. Wouters, Susanne Hoffmann-Eifert, Dan Buca, Rainer Waser, and Vikas Rana. "Forming-free metal-oxide ReRAM by oxygen ion implantation process." In Electron Devices Meeting (IEDM), 2016 *IEEE International*, pp. 4-4. IEEE, 2016.

[7] Srour, J. R., Cheryl J. Marshall, and Paul W. Marshall. "Review of displacement damage effects in silicon devices." *IEEE Transactions on Nuclear Science* 50, no. 3 (2003): 653-670.

[8] Zhang, Lijie, Ru Huang, Dejin Gao, Pan Yue, Poren Tang, Fei Tan, Yimao Cai, and Yangyuan Wang. "Total Ionizing Dose (TID) Effects on TaOx-Based Resistance Change Memory." *IEEE Transactions on Electron Devices* 58, no. 8 (2011): 2800-2804.

[9] Holt, Joshua S., Karsten Beckmann, Zahiruddin Alamgir, Jean Yang-Scharlotta, and Nathaniel C. Cady. "Effect of Displacement Damage on Tantalum Oxide Resistive Memory." *MRS Advances* (2017): 1-7.

[10] Fang, Runchen, Yago Gonzalez Velo, Wenhao Chen, Keith E. Holbert, Michael N. Kozicki, Hugh Barnaby, and Shimeng Yu. "Total ionizing dose effect of γ-ray radiation on the switching characteristics and filament stability of HfOx resistive random access memory." *Applied Physics Letters* 104, no. 18 (2014): 183507

---

[11] Bi, J. S., Z. S. Han, E. X. Zhang, M. W. McCurdy, R. A. Reed, R. D. Schrimpf, D. M. Fleetwood et al. "The Impact of X-Ray and Proton Irradiation on HfO2/Hf Based Bipolar Resistive Memories." *IEEE Transactions on Nuclear Science* 60, no. 6 (2013): 4540-4546.

[12] Liu, Qi, Ming Liu, Shibing Long, Wei Wang, Manhong Zhang, Qin Wang, and Junning Chen. "Improvement of resistive switching properties in ZrO 2-based ReRAM with implanted metal ions." *In Solid State Device Research Conference*, 2009. ESSDERC'09. Proceedings of the European, pp. 221-224. IEEE, 2009.

[13] Wang, Zhongrui, W. G. Zhu, A. Y. Du, L. Wu, Z. Fang, Xuan Anh Tran, W. J. Liu, K. L. Zhang, and H-Y. Yu. "Highly Uniform, Self-Compliance, and Forming-Free ALD HfO2-Based RRAM With Ge Doping." *IEEE Transactions on electron devices* 59, no. 4 (2012): 1203-1208.

[14] Kim, Wonjoo, Alexander Hardtdegen, Christian Rodenbücher, Stephan Menzel, Dirk J. Wouters, Susanne Hoffmann-Eifert, Dan Buca, Rainer Waser, and Vikas Rana. "Forming-free metal-oxide ReRAM by oxygen ion implantation process." In Electron Devices Meeting (IEDM), 2016 IEEE International, pp. 4-4. *IEEE*, 2016.

[15] Ascoli, Alon, Ronald Tetzlaff, Leon O. Chua, John Paul Strachan, and Richard Stanley Williams. "History erase effect in a non-volatile memristor." I*EEE Transactions on Circuits and Systems* I: Regular Papers 63, no. 3 (2016): 389-400.

[16] Neamen, Donald A. Semiconductor physics and devices. Vol. 3. New York: McGraw-Hill, 1997.

---

[17] Gusev, E. P., C. Cabral Jr, M. Copel, C. D'emic, and M. Gribelyuk. "Ultrathin HfO2 films grown on silicon by atomic layer deposition for advanced gate dielectrics applications." *Microelectronic Engineering* 69, no. 2-4 (2003): 145-151.

[18] He, G., M. Liu, L. Q. Zhu, M. Chang, Q. Fang, and L. D. Zhang. "Effect of postdeposition annealing on the thermal stability and structural characteristics of sputtered HfO2 films on Si (1 0 0)." *Surface Science* 576, no. 1-3 (2005): 67-75.

[19] Cho, M-H., Y. S. Roh, C. N. Whang, K. Jeong, S. W. Nahm, D-H. Ko, Jong Heun Lee, N. I. Lee, and K. Fujihara. "Thermal stability and structural characteristics of HfO 2 films on Si (100) grown by atomic-layer deposition." *Applied physics letters* 81, no. 3 (2002): 472-474.

[20] Goncharova, L. V., M. Dalponte, T. Feng, T. Gustafsson, E. Garfunkel, P. S. Lysaght, and G. Bersuker. "Diffusion and interface growth in hafnium oxide and silicate ultrathin films on Si (001)." *Physical Review* B 83, no. 11 (2011): 115329.

[21] Sinha, H., H. Ren, M. T. Nichols, J. L. Lauer, M. Tomoyasu, N. M. Russell, G. Jiang et al. "The effects of vacuum ultraviolet radiation on low-k dielectric films." *Journal of Applied Physics*112, no. 11 (2012): 111101.

[22] Plummer, James D. Silicon VLSI technology: fundamentals, practice and modeling. Pearson Education India, 2009.

[23] Kumar, Suhas, Ziwen Wang, Xiaopeng Huang, Niru Kumari, Noraica Davila, John Paul Strachan, David Vine, AL David Kilcoyne, Yoshio Nishi, and R. Stanley Williams. "Oxygen migration during resistance switching and failure of hafnium oxide memristors." *Applied Physics Letters* 110, no. 10 (2017): 103503.

[24] Chen, Yang Yin, Ludovic Goux, Sergiu Clima, Bogdan Govoreanu, Robin Degraeve, Gouri Sankar Kar, Andrea Fantini, Guido Groeseneken, Dirk J. Wouters, and Malgorzata Jurczak. "Endurance/retention trade-off on HfO2/metal cap 1T1R bipolar RRAM." *IEEE Trans Electron Devices* 60 (2013): 1114.

[25] Chen, Yang Yin, Robin Degraeve, Sergiu Clima, Bogdan Govoreanu, Ludovic Goux, Andrea Fantini, Gouri Sankar Kar et al. "Understanding of the endurance failure in scaled HfO2-based 1T1R RRAM through vacancy mobility degradation." In Electron Devices Meeting (IEDM), 2012 *IEEE International*, pp. 20-3. IEEE, 2012.

[26] Wong, H-S. Philip, Heng-Yuan Lee, Shimeng Yu, Yu-Sheng Chen, Yi Wu, Pang-Shiu Chen, Byoungil Lee, Frederick T. Chen, and Ming-Jinn Tsai. "Metal–oxide RRAM." *Proceedings of the IEEE* 100, no. 6 (2012): 1951-1970.

[27] Chen, B., Y. Lu, B. Gao, Y. H. Fu, F. F. Zhang, P. Huang, Y. S. Chen et al. "Physical mechanisms of endurance degradation in TMO-RRAM." In Electron Devices Meeting (IEDM), 2011 *IEEE International*, pp. 12-3. IEEE, 2011.

[28] Huang, P., B. Chen, Y. J. Wang, F. F. Zhang, L. Shen, R. Liu, L. Zeng et al. "Analytic model of endurance degradation and its practical applications for operation scheme optimization in metal oxide based RRAM." In Electron Devices Meeting (IEDM), 2013 *IEEE International*, pp. 22-5. IEEE, 2013.

[29] Huang, P., B. Chen, Y. J. Wang, F. F. Zhang, L. Shen, R. Liu, L. Zeng et al. "Analytic model of endurance degradation and its practical applications for operation scheme optimization in metal oxide based RRAM." In Electron Devices Meeting (IEDM), 2013 *IEEE International*, pp. 22-5. IEEE, 2013.

[30] D. M. Fleetwood, R. D. Schrimpf, J. G. Hong, G. Lucovsky, J. R. Schwank, and M. R. Shaneyfelt. "Total-dose radiation response of hafnium-silicate capacitors." *IEEE Transactions on Nuclear Science* 49, no. 6 (2002): 3191-3196.

[31] Butcher, Brian, Xiaoli He, Mengbing Huang, Yan Wang, Qi Liu, Hangbing Lv, Ming Liu, and Wei Wang. "Proton-based total-dose irradiation effects on Cu/HfO2: Cu/Pt ReRAM devices." *Nanotechnology* 21, no. 47 (2010): 475206.

[32] Gao, B., S. Yu, N. Xu, L. F. Liu, B. Sun, X. Y. Liu, R. Q. Han, J. F. Kang, B. Yu, and Y. Y. Wang. "Oxide-based RRAM switching mechanism: A new ion-transport-recombination model." In Electron Devices Meeting, 2008. IEDM 2008. *IEEE International*, pp. 1-4. IEEE, 2008.

---

[33] Duncan, D., Magyari-Köpe, B. and Nishi, Y., 2016. Hydrogen doping in HfO2 resistance change random access memory. *Applied Physics Letters*, 108(4), p.043501.

[34] Fang, Z., H. Y. Yu, W. J. Liu, Z. R. Wang, X. A. Tran, B. Gao, and J. F. Kang. "Temperature Instability of Resistive Switching on HfOx-Based RRAM Devices." *IEEE Electron Device Letters* 31, no. 5 (2010): 476-478.

[35] Gao, B., J. F. Kang, H. W. Zhang, B. Sun, B. Chen, L. F. Liu, X. Y. Liu et al. "Oxide-based RRAM: Physical based retention projection." In Solid-State Device Research Conference (ESSDERC), 2010 *Proceedings of the European*, pp. 392-395. IEEE, 2010.

[36] Yu, Shimeng, Ximeng Guan, and H-S. Philip Wong. "Conduction mechanism of TiN/HfOx/Pt resistive switching memory: A trap-assisted-tunneling model." *Applied Physics Letters* 99, no. 6 (2011): 063507.

[37] Walczyk, Christian, Damian Walczyk, Thomas Schroeder, Thomas Bertaud, Małgorzata Sowinska, Mindaugas Lukosius, Mirko Fraschke et al. "Impact of Temperature on the Resistive Switching Behavior of Embedded HfO_2 Based RRAM Devices." *IEEE transactions on electron devices* 58, no. 9 (2011): 3124-3131.

[38] Wang, Zhongrui, W. G. Zhu, A. Y. Du, L. Wu, Z. Fang, Xuan Anh Tran, W. J. Liu, K. L. Zhang, and H-Y. Yu. "Highly Uniform, Self-Compliance, and Forming-Free ALD HfO2Based RRAM with Ge Doping." *IEEE Transactions on electron devices* 59, no. 4 (2012): 1203-1208.

---

[39] Zhang, Haowei, Bin Gao, Bing Sun, Guopeng Chen, Lang Zeng, Lifeng Liu, Xiaoyan Liu et al. "Ionic doping effect in ZrO 2 resistive switching memory." *Applied Physics Letters* 96, no. 12 (2010): 123502.

[40] Gao, Bin, Haowei Zhang, Bing Chen, Lifeng Liu, Xiaoyan Liu, Ruqi Han, Jinfeng Kang et al. "Modeling of retention failure behavior in bipolar oxide-based resistive switching memory." *IEEE Electron Device Letters* 32, no. 3 (2011): 276-278.

[41] Chen, Fen, and Michael Shinosky. "Soft breakdown characteristics of ultralow-k time-dependent dielectric breakdown for advanced complementary metal-oxide semiconductor technologies." *Journal of Applied Physics* 108, no. 5 (2010): 054107.

[42] Moazzami, Reza, Jack C. Lee, and Chenming Hu. "Temperature acceleration of time-dependent dielectric breakdown." *IEEE Transactions on Electron Devices* 36, no. 11 (1989): 2462-2465.

[43] Cester, Andrea, Leonardo Bandiera, Marco Ceschia, Gabriella Ghidini, and Alessandro Paccagnella. "Noise characteristics of radiation-induced soft breakdown current in ultrathin gate oxides." *IEEE Transactions on Nuclear Science* 48, no. 6 (2001): 2093-2100.

[44] Minford, W. "Accelerated life testing and reliability of high K multilayer ceramic capacitors." *IEEE Transactions on Components*, Hybrids, and Manufacturing Technology 5, no. 3 (1982): 297-300.

---

[45] Moazzami, Reza, Jack C. Lee, and Chenming Hu. "Temperature acceleration of time-dependent dielectric breakdown." *IEEE Transactions on Electron Devices* 36, no. 11 (1989): 2462-2465.

Chapter VI. Summary and Conclusions.

A. Comparison of experiment with theory.

The TRIM code simulation results showed that for low-energy exposure, more protons are seen to stay in the HfO_2 film. However, 300-keV protons have enough energy so that most of them can pass through the HfO_2 film. The simulation results for vacancies distribution (Chapter III, Figure 1), show that more vacancies are generated in the HfO_2 film after 10-keV proton irradiation than 300-keV irradiation. It must be noted that these results are only those obtained for blanket films, not for the RRAM Cells themselves. However, it was seen that the damage that was produced by the 300-keV protons is more severe that that produced by the lower energy protons. This was seen because it was not possible to recover the damage from the 300-keV protons, while that produced by the 10-keV protons could be significantly recovered.

Electron-spin resonance measurements were made with the 5-nm ALD HfO_2 blanket film. The ESR spectra of pristine and-proton irradiated samples were fitted using a Gaussian distribution to determine the g values for each defect in the dielectric film. As shown in Figure 28 in chapter IV, only Si dangling bonds were detected in the pristine HfO_2 film. On the other hand, two defect states were detected in the proton-irradiated film: (1) Si dangling bonds and (2) oxygen vacancies. These results show that oxygen vacancies are generated during proton irradiation. In addition, the defect concentration of oxygen vacancies in the 10-keV proton-irradiated samples is higher than the 300-keV proton irradiated sample. This can be seen from the fitting results for oxygen

vacancies shown in Figure 28 (b) and (c) in chapter V. These results are consistent with the TRIM code simulation results as shown in Chapter III. That is, more oxygen vacancies are generated in the HfO_2 film after 10-keV proton radiation than 300-keV. For low-energy exposure, more protons are likely to stay in the HfO_2 film than the 300-keV protons which have enough energy to pass through the HfO_2 film and get to the substrate.

This results can explain the fact that some of the 10-keV proton exposed RRAM cells are formed during radiation. Low-energy proton radiation is more likely to induce a soft breakdown in the dielectric film.[1] The radiation-induced soft breakdown in high-k oxides results if the proton ions create a random conductive path in the oxide.[2] Such a soft breakdown is not, however, permanent.[2] It can indeed be recovered during resistive switching.[3] During the reset process, some radiation-induced oxygen-vacancy-interstitials can recombine under the influence of an electric field. From the results of Task one in chapter V, those RRAM cells that are formed by proton irradiation could be reset and turn to HRS. When a RRAM cell is reset from LRS to HRS, that means the oxygen vacancies have recombined with oxygen ions.

C-V measurements were made on 5 and 100-nm thick HfO_2 blanket films with a MOS structure. Figure 15 in chapter IV shows that there is a lateral leftward shift in the C-V curve of the 10-keV proton irradiated sample. The left shift means that there are fixed defect states, which are positively charged, are generated in the oxide after proton irradiation.[4] Except for the flat-band voltage shift, there is a slope in the C-V curve change after proton-irradiation. The “distorted” C-V curve (Figure 15 in chapter IV) of the proton-irradiated sample shows that interface traps are present after proton

irradiation.[5] These interface traps behave very much like bulk deep-level traps and can have energy levels in the bandgap of the oxide.[5]

The C-V characteristics of 100-nm HfO_2 samples show that the value of oxide capacitance C_{ox} is about the same before and after proton irradiation. The value of C_{ox} under reverse bias shows a 50% decrease of the 5-nm HfO_2 film capacitance after 10-keV proton exposure. Thus, the decrease of C_{ox} in the 5-nm HfO_2 samples after proton irradiation is likely from the fact that a thin layer of oxide is generated in the HfO_2/Si interface after proton irradiation (as shown in Figure 14, chapter IV). In the 100-nm HfO_2. Since the thickness of this HfO_2 film is much larger, such a change in the interface is not likely to affect the net capacitance. Therefore, the value of C_{ox} in the 100-nm HfO_2 sample is about the same after proton irradiation. Leakage-current measurements were also made with the same MOS structure. The leakage current of the 5-nm blanket films decreased after 10-keV proton irradiation, indicating that the conductance decreases. However, the leakage current of the 100-nm blanket film did not change before and after proton radiation. This indicates that both the changes in capacitance and conductance occur at the interface of the films with the electrodes.

B. Conclusions

The hypothesis of this work is that proton radiation with energies from 10-300keV will generate damage to HfO_2-based RRAM that will affect the RRAM cell's resistive switching, reliability, stability and endurance as a function of proton energy and fluence. We further

hypothesized that this damage is generated by radiation-induced atomic displacement. The effect of proton radiation on HfO_2 blanket films and HfO_2 based RRAM was investigated using 10, 100 and 300-keV protons with fluences from 10^9 to 10^{15} cm^{-2}. The I-V characteristics, endurance and retention were measured before and after irradiation.

Tasks to prove the hypothesis:

Task One: Measure RRAM cells' I-V characteristics after proton irradiation to determine whether the proton irradiated RRAM cells are still working. I-V measurements are used to determine the effect of proton radiation on the RRAM's resistive switching characteristics. These are: the HRS and LRS resistances, the forming process, and the set and reset voltages. These will be measured as function of proton energy and proton fluence. In order to find out whether the damage can be recovered, the HRS and LRS resistance of proton irradiated RRAMs will be measured immediately after after irradiation and also after 5 months' storage at room temperature.

Task Two: If the RRAM cells are still working functionally after proton radiation, then reliability tests will be made. In order to determine the effect of proton radiation on the reliability of RRAM, endurance and retention will be measured. These quantities are key parameters for memory reliability.[6]

Task Three: To measure the stability of the irradiated RRAM cells, the HRS and LRS resistance values (the ratio of HRS resistance to LRS resistance, which is often called the R_{off}/R_{on} ratio) of the proton-irradiated RRAM cells will be measured as a function of the number of switching cycles. This is because switching failures could happen when the R_{on}/R_{off} ratio is too low (< 10).[7]

Task Four: The performance of RRAM is temperature dependent,[8,9] and because proton-induced damage will be enhanced at high temperatures, the resistive switching characteristics, HRS and LRS resistances, and the endurance of proton-irradiated RRAMs will be measured as a function of temperature from room temperature to 150°C, in order to find out how the proton-irradiated RRAM cells behave at high temperature.

Task Five: To determine the cause of the damage, C-V, XRD and ESR measurements will be made on HfO_2 blanket films, to be compared with the results of a TRIM simulation. The TRIM simulation will show where displacement damage is predicted. ESR measurements will be made to determine whether displacement damage and oxygen vacancies are generated by the radiation. C-V measurements will be made to determine the radiation-induced defect-charge type and where the defects are generated. If the results of these measurements agree with each other, then it is more likely to prove the hypothesis that the damages are from radiation-induced displacement.

Tasks one to four are all made with RRAM devices, task five is made with blanket film.

The results of task one:

The proton irradiated RRAM devices work functionally after proton irradiation. However, a number of the low-energy proton-exposed samples were found to be set to LRS after exposure. In addition, after negative DC bias reset, these particular devices can switch to HRS. This forming/set process could be explained as radiation-induced dielectric soft breakdown.[10] That is, oxygen vacancies are generated during proton radiation which produces the dielectric soft breakdown. The results in a random conductive path in the oxide and switches the RRAM cell to

LRS.[11] The ESR measurements shows that a soft-dielectric breakdown results from displacement damage.

In addition, the HRS resistance value exhibited a significant decrease after irradiation. Those radiation-induced defects that could not recovered during the reset action act as temporary trapping centers and affect the conductive filaments' size.[12] [13] [14] In addition, in the HRS, there are more oxygen vacancies in the gap region of the conductive filaments. The extra oxygen vacancies can help to reconnect the filament under the set operation electric field. The resistance is related to the size of the conductive filaments.[14] Since the radiation-induced oxygen vacancies increase the size of the conductive filaments, the resistance at HRS decreased after proton irradiation. After a period of time at room temperature, the radiation-induced damage in the HfO_2 film recovered and the HRS resistance increased compared to the just-exposed samples. Once defects are formed by incident radiation, those defects will reorder to form more stable configurations which have the lowest energy levels. However, the HRS resistance is still lower than that for pristine RRAM. This indicates that the oxygen vacancies generated during proton irradiation can only be partly annealed at room temperature. After the room temperature "annealing", the HRS resistance was measured as a function of proton energy and fluence. The results show that the HRS resistance is lower with higher proton energy and higher fluence. This means that even more oxygen vacancies are generated during proton radiation, most of the could be recombined with oxygen ion during reset process and after 5 months' storage at room temperature. Those damages that are not be able to recover, act as temporary trapping centers and add extra energy in the band gap. In addition, the activation energy of oxygen vacancies is lower after proton radiation. It also decreases more with higher proton energy. Another reason is that even fewer protons stay in the HfO_2 film when energy

is 300keV, so one 300keV proton may produce more oxygen vacancies or other charged trap centers that are not be able to recovered during switching process. Therefore, there are more long-lasting damage generated with higher proton energy and fluence.

These results prove the hypothesis that proton radiation will affect the I-V characteristics of RRAM cells. However, more long-lasting damage is generated by higher proton energy and higher proton fluence.

The results of task two and three:

The results of task one show that the RRAM cells are still working functionally after radiation. Good uniformity (small variance) of switching parameters such as LRS and HRS resistance were then measured in pristine RRAM cells. Within 10^6 switching cycles, there was no significant decrease of the ON/OFF (R_{HRS}/R_{LRS}) ratio (also called the logic window) seen in the pristine RRAM cells. The proton-exposed RRAM cells were exposed to different proton energies with the same fluence (10^{14} cm^{-2}). After proton irradiation with energies from 10 to 300keV, the endurance decreases, especially the 50% endurance failure. In addition, the 50% endurance failure decreases (RRAM cells breakdown with fewer switching cycles) with higher proton energies. For the pristine RRAM samples, 50% of the cells failed below 300k cycles. 50% of the 300keV proton irradiated RRAM cells failed below 100k cycles, around 50% of the 100keV and 10keV proton irradiated RRAM cells failed below 180k cycles. Even though the endurance of proton irradiated RRAM is not as long as that for pristine RRAM, the endurance of proton irradiated RRAM cells shows that a small fraction of them can still get up to 10^6 cycles. The endurance was also measured as a function of fluence. RRAM cells were exposed with a proton energy of 100keV and different

proton fluences: 10^{9}, 10^{11}, 10^{13}, 10^{14} and 10^{15} cm^{-2}. When the fluence was less than 10^{13} cm^{-2}, the endurance was not significantly affected by the proton radiation, the endurance is very close to pristine samples. However, when the fluence was higher than 10^{13} cm^{-2}, the endurance decreased compared with the pristine RRAM cells, as the values showed in Table 4, Chapter V.

The radiation-induced defects in the RRAM devices may affect the CFs' size, length and filament growth activation energy E_a.[15] The larger CFs sizes may cause reset failure.[16] The uncombined proton-induced oxygen vacancies and defects serve as electron trapping centers in the HfO_2 film and make the dielectric material easier to break down.[11] In addition, H ions can reduce the filament formation energy. The higher the energy of the protons, the more reduction in the formation energy was observed.[17] Therefore, the endurance cycles of proton irradiated RRAM consistently decreased with higher proton energy.

The results of Task four:

The endurance of pristine and proton irradiated RRAM cells were also measured at high temperatures, *i.e.*, 75, 120 and 150°C. The endurance of pristine RRAM cells decreased as the temperature increased. For endurance cycles below 100k, more devices failed at higher temperatures. It was also observed that the HRS current increases at high temperature. With increasing temperature, the probability of oxygen vacancy formation increases. The increased oxygen vacancy-related-traps density at high temperature can enhance the trap-assisted tunneling current at HRS.[18, 19] In addition, oxygen-ion mobility will increase with increasing temperature.[20] The probability of creating oxygen vacancies as well as the oxygen-ion mobility both *increase* at higher temperatures. This shows that the set and reset voltage should *decrease* with increasing

temperature which has been observed in Figure 22, chapter V. High-temperature endurance measurements were also made with proton-irradiated RRAM cells. The 10 and 100-keV proton-irradiated RRAM cells' endurance cycles decreased at higher temperatures. The degradation of endurance at high temperature is less significant in the RRAM cells that were exposed with higher energy photons (at the same fluence). However, the endurance of 300-keV proton-exposed RRAM cells measured at high and room temperature are very close, except that it was seen that more 300-keV proton-irradiated RRAM cells failed before 50k switching cycles at 150°C compared with the lower temperature 300keV case.

As shown in the preliminary work, the HRS resistance decreases with higher proton energy. This means that during resistive switching, there are more unrecoverable radiation-induced defects in 300-keV proton-irradiated RRAM cells than at lower proton energies. These defects enhanced electron hopping and decreased the activation energy E_a.[21, 22]

Based on crystal defect and probability theories, the cumulative failure probability can be expressed as a function of defect generation probability $\mathrm{F} = 1 - (1 - p)^{at}$, where p is the defect generation probability: $\mathrm{p} \propto \exp\left(-\frac{E_a}{k_B \mathrm{T}}\right)$.[23, 24, 25] A low E_a value shows a weak temperature dependence of the dielectric breakdown.[26] Since the E_a value is smaller after higher-energy proton irradiation,[17] the 300-keV proton irradiated RRAM cells have the smallest E_a value. However, more oxygen vacancies are generated in 10-keV exposed RRAM cells than in 300-keV. However, most of the proton-induced oxygen vacancies can be recovered during the reset process using an electric field, because these damages are like the soft breakdown in dielectrics that can be recovered. However, those damages that are not be able to recovered during reset appear in lower

values for the HRS resistance and E_a. This explains the results that the endurance of higher-energy exposed RRAM cells showed fewer differences between the measurements at different temperatures, as showed in Figure 23, chapter V.

The LRS retention was measured for pristine, 10, 100 and 300-keV proton-exposed RRAM cells at 120°C. The retention measurements is the time that the device at least could work before breakdown, so the samples exposed to the highest proton fluence (10^{15} cm^{-2}) were used in the retention measurement. All the measured RRAM cells could still be set and reset after >10^5 s (more than 8 hours) retention measurement. These results show that after proton exposure, the RRAM cells still have very good retention behavior. The 8-hour retention time measured in this situation can be extrapolated to about 14-15 years' lifetime.[27]

The results of task five (measured with blanket films):

The ESR measurement results for blanket films show that, during proton irradiation, oxygen vacancies are generated in the HfO_2 blanket films. During 10-keV proton radiation, more oxygen vacancies were generated in the HfO_2 films than when they were irradiated with 300-keV protons. This result is constant with the TRIM simulation results. The C-V measurements also showed that positively charged defects were generated in the HfO_2/Si interface and dielectric bulk. The XRD measurements made within a week and 5 months after proton radiation shows that the proton radiation did not change the crystalline structure of the HfO_2 film.

These results prove the hypothesis that the effects on RRAM cells are caused by radiation induced oxygen vacancies that is generated from displacement damage.

C. Future work

One of the limiting factors of RRAM is the need for an initial electroforming step to create a conductive filament in the dielectric. The forming process is a timing-consuming step. In addition, the forming voltage, which is much higher than the switching voltage (set and reset voltage), makes RRAM less compatible with low-voltage CMOS technology. [28] Therefore, it is important to reduce the forming voltage as low as the set voltage or to have forming-free RRAM. From this work, it has been found that some of the RRAM cells were formed during 10-keV proton irradiation. As a possibility to extend the work, in the right energy range, proton radiation could be used to get forming-free HfO_2-based RRAM devices. The optimized proton energy range and fluence need to be determined to produce forming-free RRAM devices, without degrading the switching performances and endurance.

An improvement of resistive switching properties in ZrO_2 based RRAM with implanted ion has been reported.[29] After doping Ti in ZrO_2, the variations of set voltage and HRS resistance could be reduced. In this work, the HfO_2-based RRAM shows more variations of HRS resistance after proton radiation and/or at higher temperature. Future work to find an ion implantation process that can reduce such variations is important.

References

[1] Zhang, Haowei, Bin Gao, Bing Sun, Guopeng Chen, Lang Zeng, Lifeng Liu, Xiaoyan Liu et al. "Ionic doping effect in ZrO 2 resistive switching memory." *Applied Physics Letters* 96, no. 12 (2010): 123502.

[2] Felix, J. A., J. R. Schwank, Daniel M. Fleetwood, M. R. Shaneyfelt, and Evgeni P. Gusev. "Effects of radiation and charge trapping on the reliability of high-κ gate dielectrics." *Microelectronics Reliability* 44, no. 4 (2004): 563-575.

[3] Ribes, G., J. Mitard, M. Denais, S. Bruyere, F. Monsieur, C. Parthasarathy, E. Vincent, and Ge Ghibaudo. "Review on high-k dielectrics reliability issues." *IEEE Transactions* on Device and materials Reliability 5, no. 1 (2005): 5-19.

[4] Sinha, H., H. Ren, M. T. Nichols, J. L. Lauer, M. Tomoyasu, N. M. Russell, G. Jiang et al. "The effects of vacuum ultraviolet radiation on low-k dielectric films." *Journal of Applied Physics112*, no. 11 (2012): 111101.

[5] Plummer, James D. Silicon VLSI technology: fundamentals, practice and modeling. Pearson Education India, 2009.

---

[6] Wong, H-S. Philip, Heng-Yuan Lee, Shimeng Yu, Yu-Sheng Chen, Yi Wu, Pang-Shiu Chen, Byoungil Lee, Frederick T. Chen, and Ming-Jinn Tsai. "Metal–oxide RRAM." *Proceedings of the IEEE* 100, no. 6 (2012): 1951-1970.

[7] Chen, Yang Yin, Robin Degraeve, Sergiu Clima, Bogdan Govoreanu, Ludovic Goux, Andrea Fantini, Gouri Sankar Kar et al. "Understanding of the endurance failure in scaled HfO2-based 1T1R RRAM through vacancy mobility degradation." In Proc. IEEE Electron Devices Meeting (IEDM), 2012 *IEEE International*, pp. 20-3. IEEE, 2012.

[8] Walczyk, Christian, Damian Walczyk, Thomas Schroeder, Thomas Bertaud, Małgorzata Sowinska, Mindaugas Lukosius, Mirko Fraschke et al. "Impact of Temperature on the Resistive Switching Behavior of Embedded HfO2-Based RRAM Devices." *IEEE transactions on electron devices* 58, no. 9 (2011): 3124-3131.

[9] Fang, Z., H. Y. Yu, W. J. Liu, Z. R. Wang, X. A. Tran, B. Gao, and J. F. Kang. "Temperature Instability of Resistive Switching on HfOxBased RRAM Devices." *IEEE Electron Device Letters* 31, no. 5 (2010): 476-478.

[10] Zhang, Haowei, Bin Gao, Bing Sun, Guopeng Chen, Lang Zeng, Lifeng Liu, Xiaoyan Liu et al. "Ionic doping effect in ZrO 2 resistive switching memory." *Applied Physics Letters* 96, no. 12 (2010): 123502.

---

[11] Felix, J. A., J. R. Schwank, Daniel M. Fleetwood, M. R. Shaneyfelt, and Evgeni P. Gusev. "Effects of radiation and charge trapping on the reliability of high-κ gate dielectrics." *Microelectronics Reliability* 44, no. 4 (2004): 563-575.

[12] Srour, J. R., Cheryl J. Marshall, and Paul W. Marshall. "Review of displacement damage effects in silicon devices." *IEEE Transactions on Nuclear Science* 50, no. 3 (2003): 653-670.

[13] Zhang, Lijie, Ru Huang, Dejin Gao, Pan Yue, Poren Tang, Fei Tan, Yimao Cai, and Yangyuan Wang. "Total Ionizing Dose (TID) Effects on TaOx-Based Resistance Change Memory." *IEEE Transactions on Electron Devices* 58, no. 8 (2011): 2800-2804.

[14] Holt, Joshua S., Karsten Beckmann, Zahiruddin Alamgir, Jean Yang-Scharlotta, and Nathaniel C. Cady. "Effect of Displacement Damage on Tantalum Oxide Resistive Memory." *MRS Advances* (2017): 1-7.

[15] Butcher, Brian, Xiaoli He, Mengbing Huang, Yan Wang, Qi Liu, Hangbing Lv, Ming Liu, and Wei Wang. "Proton-based total-dose irradiation effects on Cu/HfO2O2O2: Cu/Pt ReRAM devices." *Nanotechnology* 21, no. 47 (2010): 475206.

[16] Gao, B., S. Yu, N. Xu, L. F. Liu, B. Sun, X. Y. Liu, R. Q. Han, J. F. Kang, B. Yu, and Y. Y. Wang. "Oxide-based RRAM switching mechanism: A new ion-transport-recombination model." In Electron Devices Meeting, 2008. IEDM 2008. *IEEE International*, pp. 1-4. IEEE, 2008.

[17] Duncan, D., Magyari-Köpe, B. and Nishi, Y., 2016. Hydrogen doping in HfO2O2O2 resistance change random access memory. *Applied Physics Letters*, 108(4), p.043501.

[18] Yu, Shimeng, Ximeng Guan, and H-S. Philip Wong. "Conduction mechanism of TiN/HfOx/Pt resistive switching memory: A trap-assisted-tunneling model." *Applied Physics Letters* 99, no. 6 (2011): 063507.

[19] Walczyk, Christian, Damian Walczyk, Thomas Schroeder, Thomas Bertaud, Małgorzata Sowinska, Mindaugas Lukosius, Mirko Fraschke et al. "Impact of Temperature on the Resistive Switching Behavior of Embedded HfO_2 Based RRAM Devices." *IEEE transactions on electron devices* 58, no. 9 (2011): 3124-3131.

[20] Butcher, Brian, Xiaoli He, Mengbing Huang, Yan Wang, Qi Liu, Hangbing Lv, Ming Liu, and Wei Wang. "Proton-based total-dose irradiation effects on Cu/HfO_2: Cu/Pt ReRAM devices." *Nanotechnology* 21, no. 47 (2010): 475206.

[21] Wang, Zhongrui, W. G. Zhu, A. Y. Du, L. Wu, Z. Fang, Xuan Anh Tran, W. J. Liu, K. L. Zhang, and H-Y. Yu. "Highly Uniform, Self-Compliance, and Forming-Free ALD HfO_2 Based RRAM with Ge Doping." *IEEE Transactions on electron devices* 59, no. 4 (2012): 1203-1208.

[22] Zhang, Haowei, Bin Gao, Bing Sun, Guopeng Chen, Lang Zeng, Lifeng Liu, Xiaoyan Liu et al. "Ionic doping effect in ZrO 2 resistive switching memory." *Applied Physics Letters* 96, no. 12 (2010): 123502.

---

[23] Gao, Bin, Haowei Zhang, Bing Chen, Lifeng Liu, Xiaoyan Liu, Ruqi Han, Jinfeng Kang et al. "Modeling of retention failure behavior in bipolar oxide-based resistive switching memory." *IEEE Electron Device Letters* 32, no. 3 (2011): 276-278.

[24] Chen, Fen, and Michael Shinosky. "Soft breakdown characteristics of ultralow-k time-dependent dielectric breakdown for advanced complementary metal-oxide semiconductor technologies." *Journal of Applied Physics* 108, no. 5 (2010): 054107.

[25] Moazzami, Reza, Jack C. Lee, and Chenming Hu. "Temperature acceleration of time-dependent dielectric breakdown." *IEEE Transactions on Electron Devices* 36, no. 11 (1989): 2462-2465.

[26] Cester, Andrea, Leonardo Bandiera, Marco Ceschia, Gabriella Ghidini, and Alessandro Paccagnella. "Noise characteristics of radiation-induced soft breakdown current in ultrathin gate oxides." *IEEE Transactions on Nuclear Science* 48, no. 6 (2001): 2093-2100.

[27] Minford, W. "Accelerated life testing and reliability of high K multilayer ceramic capacitors." *IEEE Transactions on Components*, Hybrids, and Manufacturing Technology 5, no. 3 (1982): 297-300.

[28] Kim, Wonjoo, Alexander Hardtdegen, Christian Rodenbücher, Stephan Menzel, Dirk J. Wouters, Susanne Hoffmann-Eifert, Dan Buca, Rainer Waser, and Vikas Rana. "Forming-free metal-oxide ReRAM by oxygen ion implantation process." In Electron Devices Meeting (IEDM), 2016 *IEEE International*, pp. 4-4. IEEE, 2016.

---

[29] Liu, Qi, Ming Liu, Shibing Long, Wei Wang, Manhong Zhang, Qin Wang, and Junning Chen. "Improvement of resistive switching properties in ZrO 2-based ReRAM with implanted metal ions." In Solid State Device Research Conference, 2009. ESSDERC'09. *Proceedings of the European*, pp. 221-224. IEEE, 2009.